Physical Aspects of Photochemistry and Radiation Chemistry of Molecules Adsorbed on SiO_2, γ-Al_2O_3, Zeolites, and Clays

J. Kerry Thomas[1]

Department of Chemistry and Biochemistry, University of Notre Dame, Notre Dame, Indiana 46556

Received July 13, 1992 (Revised Manuscript Received October 19, 1992)

Contents

I. Introduction

The chemistry resulting from the irradiation of mobile systems e.g. gases and liquids has received detailed attention over the last 50 years. The same cannot be said of solid systems which is mainly due to the enhanced experimental difficulties often associated with opaque or powdered samples. The concept of motion in rigid systems, being different to that in liquids and gases, also tends to hamper the design of systems that produce chemistry. In spite of this detail, the industrial application of chemistry in solids (i.e. solid catalysts) and photophysical events (as in detection system) is well advanced. The last 10 years has seen increased activity in the chemistry of systems adsorbed on solids, as many analytical techniques are now available for such systems. The purpose of this review is to discuss recent photochemical studies on selected solid systems and to compare and contrast these studies with other radiation chemical studies (mostly older studies).

John Kerry Thomas was born in Wales in 1934. He attended the University of Manchester in England from 1951 to 1957, where he obtained a B.Sc. degree in 1954 and a Ph.D. in 1957. From 1957 to 1958 he was a postdoctoral fellow at the National Research Council in Ottawa, Canada. He returned to Harwell, England, as a Scientific Officer in 1958. In 1960 he joined the Argonne National Laboratory in Illinois, where he remained until 1970. In 1970 he went to the University of Notre Dame as a Professor of Chemistry. In 1969 he was awarded an honorary Doctor of Science by the University of Manchester; in 1974 he was given the research award of the Radiation Research Society; and he was a Gäst Professor at the Hahn Meitner Institute in Berlin in 1975. He was appointed Julius A. Nieuwland C.S.C. Professor of Chemistry in 1984. He is the author of 300 research papers and review articles and American Chemical Society monograph no. 181 *Chemistry of Excitation at Interfaces*.

The solid systems discussed will be porous silica, γ-alumina, zeolites, and clay systems, for the most part in the powdered or dry state. Other solid systems, TiO_2, low-temperature glasses, and colloidal particles, will be brought up as the occasion demands. A variety of classical systems will be adsorbed or coated on the above solid substrates. Low-energy irradiation or photochemical studies as well as high energy radiation or radiation chemical studies will be discussed.

II. Mechanism of Energy Loss

At this stage, it is pertinent to consider, side by side, the overall nature of the energy loss and subsequent chemistry, by both low-energy and high-energy irradiation of the samples.

Figure 1 outlines the processes that are generally accepted to occur on irradiation of a material RH. The solid lines describe the high-energy radiation events

0009-2665/93/0793-0301$12.00/0

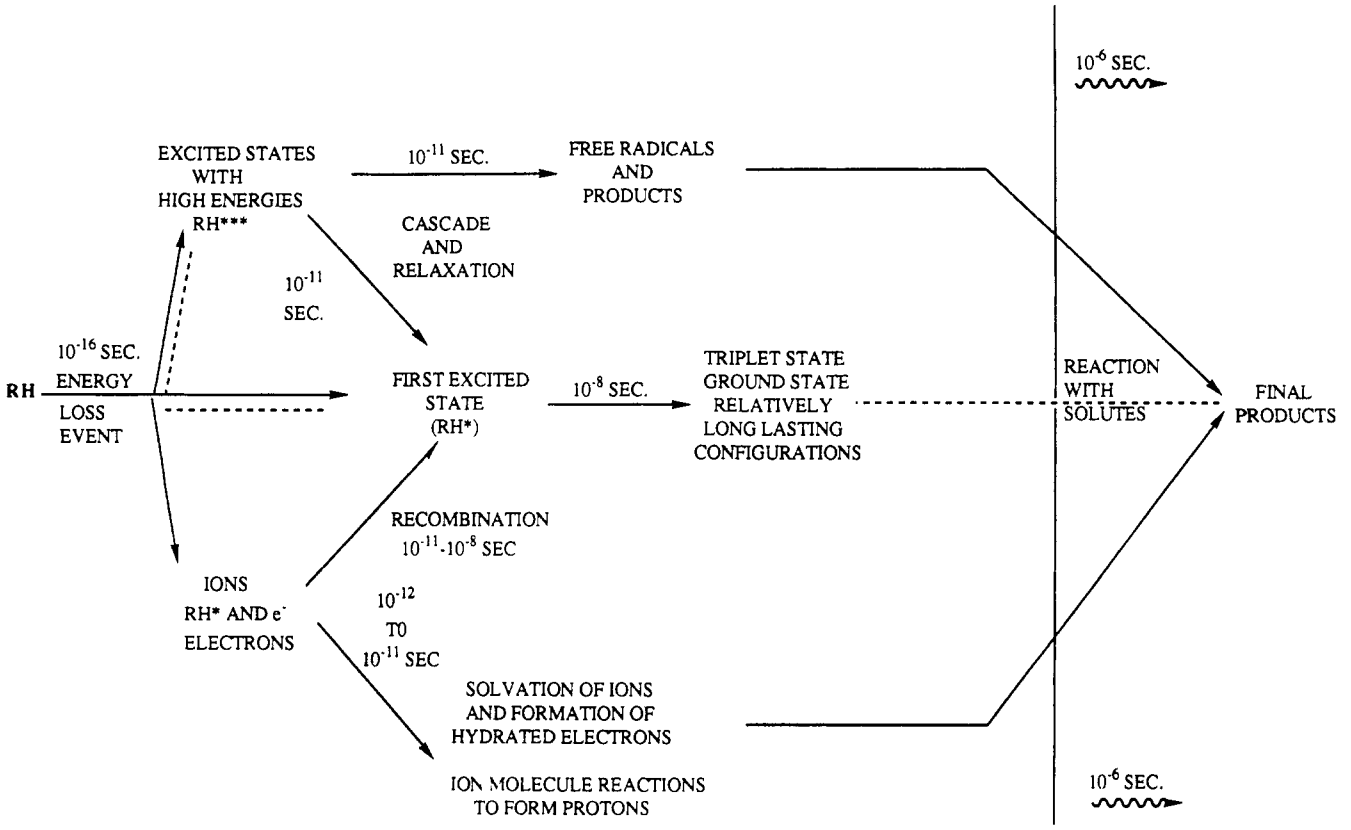

Figure 1. Time sequence of species in the high-energy irradiation of a condensed system.

and the dotted lines the events due to low-energy irradiation. The most basic difference between photochemistry and radiation chemistry is that in the former the energy is lost selectively to a chosen molecule, while in the latter the energy is lost to each component in proportion to its electron density. In photochemistry the solute is preferably excited; in radiation chemistry it is the solvent that is mainly excited.[2-5] This point becomes clearer with the details given below. The mechanism of excited states formation by low-energy radiation, or photochemistry, is well established. Excitation into the first excited state leads to long-lived species (nanosecond) which can fluoresce, intersystem cross, or produce chemistry. Excitation into states above the first excited state can lead to unique chemistry, which competes with rapid internal conversion leading to the first excited state, and the resulting chemistry is that of the first excited state. The mode of formation of excited states by high-energy radiation, or radiolysis, is still debated.[5] For a number of years the formation of excited states on radiolysis with γ-rays, fast electrons, or α-particles has been used as a method of measurement of the energy of the radiation and is the basis of the scintillation technique.[6] Various theories are used to account for the formation of the excited states. The current theory is that the radiolysis initially produces ions the rapid recombination of which results in energy appearing as both triplet and singlet excited states.[7] An alternative theory, although by no means as well established, is that of direct excitation, or the optical theory of the energy loss.[4,8] A simple calculation shows that both processes, the formation of excited states by direct excitation and also via subsequent ion recombination, could occur.[5] In practice, it is found that excited states are formed predominantly on radiolysis of nonpolar systems, or materials of low dielectric constant such as benzene or cyclohexane, while ionic products are formed on radiolysis of polar systems such as water or alcohols. In photochemistry, excitation of a material inevitably leads to the singlet excited state, and any triplet states are formed by intersystem crossing from this state. In some instances the excited triplet state can be formed directly from the singlet ground state. This spin-forbidden process is enchanced by the presence of heavy atoms e.g. I_2; excitation with higher energies can lead to ionization, and the neutralization of the ions also gives excited triplets.

Intersystem crossing from singlet excited states also occurs in radiation chemistry; however, triplet states are also formed independently of excited singlet states.[9] Nanosecond time domain studies have established that some of the triplet excited states are formed by ion recombination, which is also a possible source of singlet excited states. Picosecond studies have also shown that the mode of the formation of the excited state is by no means simple and that some of the singlet excited states and ions are formed rapidly.[10] This could be caused by an initial action of the radiation to form ions, electrons, and positive holes. Fast-ion recombination then results from electrons, which are partially trapped or are solvated in the liquid, reacting with the positive holes. Such a process is expected to be very rapid, as the electrons have high mobilities in these systems. The slow process could be due to positive holes recombining with electrons which have become trapped on solute molecules. This latter process is slower than the former as anions move at a much slower rate that electrons in these liquids. An outline of the process is shown in Figure 1.

At first sight it would appear that similar events play a major role in the radiolysis of solids, but due to their

rigidity solids freeze out much of the chemistry that occurs in local regions of high-energy release. The diffusion of reactive species, which can mask important events in mobile systems, is minimized in solid systems.[11]

III. Experimental Techniques

Steady-state irradiations are carried out with $^{60}Co\gamma$ sources for high-energy radiation and with conventional, mercury, or Xenon arc lamps for photochemical studies. Pulsed studies are carried out on a Febetron field emission accelerator[11] for high-energy studies and with a variety of conventional lasers for photochemical studies. The Febetron produces 0.5 MeV electrons in 2-ns pulses the energy being 10^5 rad/pulse; 1 rad ≡ 100 erg/gm; linear electron accelerations have been used for some of the work. The spectroscopic detection system have been described.[5]

For the most part, the solids studied are porous silica, γ-alumina, clays, and zeolites; other solids are indicated as appropriate. Molecules were adsorbed on the solids, all of which have large surface areas, from pentane or hexane solutions of the solute.[12] In some instances the molecules are sublimed onto the surfaces in vacuum.[13] Precise details of sample preparation are given in the references cited.

Pictoral representations of the solids discussed are given in Figures IV and V. The simplest case is that of silica gels.

IV. Adsorption Sites on Silica Gel

The thermal[14] and the chemical[15-17] treatments of the silica gels alter the degree of clustering of the silanol functionality present on the silica surface. It has been shown[15,18] that the geminal silanol configuration gives rise to an absorption site which when occupied by aniline yielded a protonated adsorbed form of aniline; a similar correlation would account for the observed photophysical behavior of other amines e.g. 1-aminopyrene on silica gel surfaces. Pyrenecarboxylic acid (PCA) has also been used to probe the microacidity of the silanol functionality.[19] Scheme I was established for the photophysics of PCA. In particular, the observed fluorescence decay rate constant was found to be diagnostic for the determination of the apparent pH of the microenvironment.

Scheme I

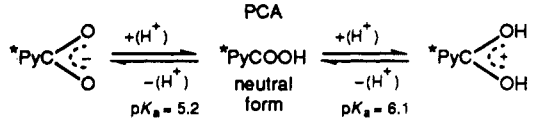

PCA adsorbed on SiO_2 from Matheson, Coleman, Bell, Co. demonstrated fluorescence of a neutral form, and FS-662 (Fisher Scientific Co.) bound PCA demonstrated fluorescence of mixed anionic/neutral forms. The observed fluorescence decay rate constants of 1.9×10^8 and 3.8×10^7 s^{-1} correspond to an apparent pH of 1.6 and 4.1 for the microenvironments of the geminal and the nongeminal silanols, respectively.

The ^{29}Si NMR,[20] cross polarization magic-angle spinning (CPMAS) and ^1H NMR magic-angle spinning with multiple-pulsed line narrowing (CRAMPS for

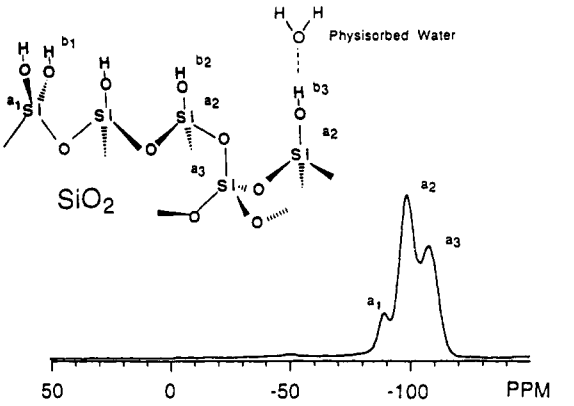

Figure 2. Different OH groupings on the SiO_2 surface and Si NMR illustrating the three groupings.

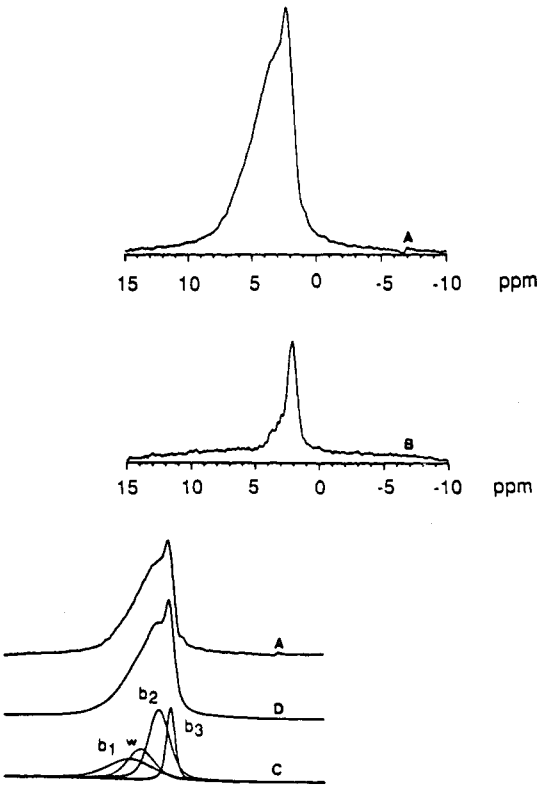

Figure 3. ^1H CRAMPS NMR of MCB silica gel.

combined rotation and multiple pulse spectroscopy) techniques of Maciel et al.[21,22] indicate that the Fisher Scientific FS-662 silica gel possesses 9% of its silanol functionality in the geminal configuration. Figure 2 presents the silanol configurations at a SiO_2 surface as on a MCB silica gel, and ^{29}Si CP/MAS NMR of the various Si in the silanol groups. The percentage of MCB surface silanol functionality in the geminal configuration is determined to be 30%. Figure 3 presents the ^1H CRAMPS NMR of the MCB silica gel sample dried under vacuum both at 100 °C along with signal deconvolution. The deconvolution clearly shows the resolution of a fourth set of transitions present with the MCB silica at 396.6 Hz not present with FS-662. The 396.6-Hz ^1H transition is interpreted as originating from the geminal silica configuration. The geminal configuration is completely, and the hydrogen-bonded vicinal configuration is partially removed by heating the MCB silica at 500 °C. The redistribution of surface silica functionality as observed by NMR support the distribution observed by photophysical probing tech-

niques. The ^1H CRAMPS NMR of the MCB silica gel yields a surface silanol functionality distribution of 30% geminal, 48% vicinal, and 22% isolated. The OH groups contribute to the adsorption capacity of the SiO_2 for arenes from alkane solution. Removal of the OH by heating, almost completely eliminates the adsorption of arenes from alkane solution.

V. Nature of Adsorption Sites on γ-Alumina

The adsorption of arenes onto γ-Al_2O_3 gives rise to complex electronic spectra which are indicative of the γ-Al_2O_3 surface. The characteristic diffuse reflectance spectra of *N,N'*-tetramethylbenzidene (TMB), adsorbed on γ-alumina surfaces (4×10^{-7} mol/g which corresponds to 3.0% monolayer coverage) consists of several absorption bands. On alumina of low pretreatment temperature T_a (T_a = 130 °C), TMB exhibits two distinct absorption bands, one at short wavelength with a peak maximum at 310 nm and the other one at longer wavelength with a maximum at 470 nm. The short wavelength absorption band is identified as the physisorbed TMB, in agreement with that of TMB in polar solvents such as methanol and water.[23a] The structured band at long wavelengths is identified as the cation radical of TMB similar to that found in photolyzed micellar solutions.[23b]

As with other metal oxides, the surface of γ-alumina is generally covered with a number of hydroxyl layers. It is known that several types of hydroxyl sites are present on the surface of γ-alumina.[24,25] Pretreatment or heating alumina at high temperatures leads to dehydroxylation of the surface hydroxyl groups and the formation of Lewis acid sites on the surface. During dehydration, OH groups which have low acidity combine with hydrogen atoms from the neighboring sites with stronger acidity, forming water molecules. This process creates an anion vacancy (Lewis acid site) which exposes coordinatively unsaturated (CUS) aluminum cations and a cation vacancy (CUS oxygen).

In earlier work, the fluorescence probing of γ-alumina with pyrene and its derivatives has demonstrated that there exists a variety of surface active sites, namely, physisorption sites, charge-transfer complex sites, and cation sites. Physisorption sites, where adsorbed molecules interact with the surface through hydroxyl groups, dominate on alumina surfaces of low pretreatment temperatures (~100 °C). The cation sites or the Lewis acid sites, which are produced from surface dehydroxylation at high pretreatment temperatures (>300 °C) are responsible for cation radical formation. The charge-transfer complex sites, which are a combination of the physisorption sites and the Lewis acid sites, are present at intermediate pretreatment temperatures.

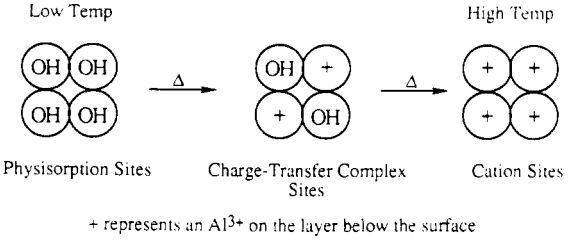

The physisorption between polyaromatic hydrocarbons and surfaces of metal oxides has been described as bonding between surface hydroxyl groups and the π-electron system of polyaromatic hydrocarbons.[26,27] However, the physisorption between TMB and surface hydroxyl groups may occur via hydrogen bonding between nonbonding electrons from nitrogen atoms and hydroxyl groups. Lewis acid sites (CUS cations) are strong electron acceptors which may accept nonbonding electrons from the nitrogen atom of a TMB molecule, thus forming a TMB cation radical (TMB^+). The structured absorption band at 470 nm of TMB on alumina is identical to that reported for TMB^+ in other systems, for example, in the irradiated micellar solution of sodium dodecyl sulfate.[23a] Cation radicals of pyrene were observed only with pyrene on alumina at high pretreatment temperatures (T_a > 450 °C) but the cation radicals of TMB were observed on alumina even at T_a = 130 °C. This is a consequence of the lower ionization potential of TMB (6.1–6.8 eV) compared to that of pyrene (7.55 eV).[28,29] The increase of the TMB cation radical (470-nm absorption band) with increasing pretreatment temperature is attributed to the larger number of the Lewis acid sites produced on higher T_a surfaces.[25] Thus the Lewis acid sites on γ-Al_2O_3 and silica alumina catalysts present active adsorption sites, which are quite distinct from the physio adsorption sites on SiO_2 gel.

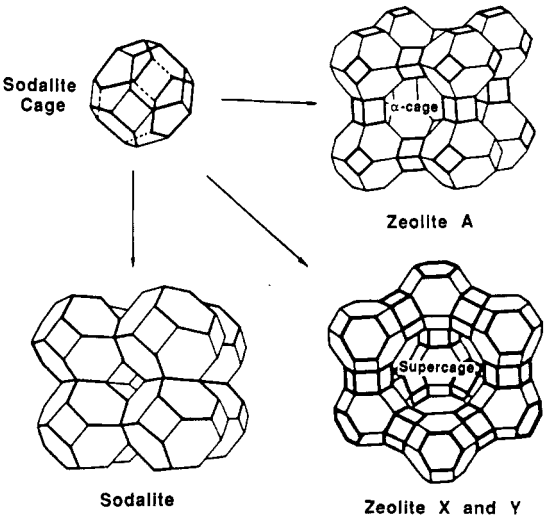

Figure 4. Diagramatic representation of zeolites.

VI. Adsorption of Molecules in Zeolites

Figure 4 shows the cages and channels found in zeolite structures, and Table I lists the parameters of these cages and channels: pore aperture, cage diameter, etc. The location and distribution of cations in these zeolites are given in the literature[31] for the original form of the zeolite, but for the Cd^{2+}-exchanged zeolites, insufficient data are available except for zeolites X and A.[32,33] However, the literature survey states that divalent cations occupy preferably the cation sites in the smaller cages rather than those in the bigger cages or channels.[31] The migration of divalent cations toward the smaller cages during dehydration often occurs if the zeolites are partially ion exchanged. Upon adsorption of guest molecules, the reverse processes could take place, depending on the experimental conditions and the strength of the interactions between the cations and the guest molecules.

Table I. Structure Parameters of Zeolites[30]

zeolite	main cage or channel	diameter (Å)	entry aperture (Å)
sodalite	sodalite cage	6.6	2.1
zeolite A	sodalite cage	6.5	2.1
	α-cage	11	4.1
zeolite X	sodalite cage	6.6	2.1
	supercage	13	7.4
chabazite	chabazite cage	6.7–10	3.7–4.2
zeolite L	cancrinite cage	2.6	2.1
	channel along [001]	7.1	7.1
offretite	gmelinite cage		3.6–5.2
	channel along [001]	6.4	
ZSM-5	channel along [010]	5.4–5.6	5.4–5.6
	channel along [100]	5.1–5.5	5.1–5.5

VII. Adsorption on Clays

The structures of various clays have been established,[34] aqueous colloid formation has been described,[35] and there is an abundance of reports on the catalytic effects of clays on chemical reactions.[36-39] Many different types of clay occur in nature. The most prominent clays in catalysis are montmorillonite, hectorite, and kaolin. The first clays are designated as 2:1 layered clays and are expandable in water, while kaolin is a 1:1 clay and nonexpendable. The expandable nature of montmorillonite and hectorite makes them particularly suitable for colloidal studies; this will emerge subsequently as the structures of the clays are outlined. Artificial clays also exist, the most prominent being laponite, which is a lithium magnesium silicate and forms excellent colloids in water. Figure 5 shows, in a diagrammatic sense, the structure of a 2:1 clay such as montmorillonite. Two clay layers are depicted in this figure. The interlayer space shown contains adsorbed cations and may also contain water. The thickness of the clay sheet is 6.6 Å from oxygen centers as shown, while the interlayer thickness can vary from several to tens of angstroms, depending on the water content of the clay and on the nature of the material absorbed in the layer. The clay consists of platelets with long dimensions of several microns and thickness 6.6 Å. In a colloidal solution, one platelet may exist alone or fused with others, giving particles consisting of several platelets. To a large degree, the nature of the aqueous solution controls the number of layers per particle.

Due to isomorphous substitution in the clay structure of one atom with another of lower valency, the clay possesses a net negative charge. The excess negative charge on the clay is balanced by the adsorption of cations on the layered surfaces. The cation exchange capacity of a clay is very high and approaches 10^{-3} equiv/g of clay. Organic cations such as cetyltrimethylammonium ion may be exchanged onto the clay to produce a hydrophobically modified clay. For the most part, neutral organic molecules such as benzidene and pyrenes are not adsorbed on aqueous clay colloids, while hydrophobically modified colloids do act as hosts for these materials. Clay, oven dried at 104 °C, adsorbs aromatic molecules from alkane solutions to at least monolayer coverages.

The 2:1 layered clays, or smectites, only achieve small interlayer spacings of several angstroms. However, large molecules may be intercalated between the clay layers, and following subsequent heat treatment, large (20 Å and greater) interlayer spacing can be achieved.[40,41] To date, little photochemistry has been reported in pillared clay systems. The need for a constant interlayer spacing will become even more important in future photochemical studies.

Dry smectite clays initially expand in the presence of water to take up one to three or four water layers in a stepwise fashion, which increases the interlayer separation to distances of 3–12 Å.[35] An aqueous clay suspension contains hydrated clay particles, each consisting of one or more individual clay sheets separated by several water layers. The absolute degree of dispersion, or the number of colloidal particles compared to the number of individual clay sheets, is in general not known, although there have been numerous investigations of aqueous dispersions of some specific clay samples.[44-47] Recently, a spectroscopic technique has been devised to monitor the degree of layering in laponite clay colloids.[47] In contact with a bulk water phase, the exchangeable cations at the clay surface have a tendency to diffuse into the bulk water, where their concentration is lower. As the diffusion of the cations proceeds, significant particle–particle repulsions develop, and this leads to dissolution or deflocculation of the clay mineral (osmotic swelling) and to formation of a colloidal suspension. Hydration forces may independently contribute to the swelling behavior of expanding clays.[48,49] The net behavior of a clay in water may be regarded as the sum of contributions from the Born repulsion, the van der Waals attraction, and the electric double-layer repulsion. The specific countercations involved (Schulze–Hardy rule), the surface charge density, and particle size all affect the degree and stability of a clay dispersion.[35,42] The clay hydrates initially formed in the presence of bulk water (three or four water layers) possess some stability, and it is usual to apply some physical agitation of the sample to enhance the dispersion of the clay.

The rheological behavior of the clay suspensions is related to the degree and nature of particle–particle aggregation and is of concern in many technological applications. However, while the viscosities and shear strength measurements provide some information about interactions between particles, it is difficult to obtain precise information about the extent of layering, since clay particle edge–edge or edge–face interactions can dominate changes in the viscosity.[35,43,44]

Recently, plate–plate particle interactions have been studied by the direct measurement of surface forces using mica crystals and aqueous montmorillonite dispersions.[42,48,49] The results suggest that the small-size fraction of lithium montmorillonite completely disperses as single sheets in water. From small-angle neutron diffraction studied and electron microscopy of lithium montmorillonite,[45,46] it was concluded that the major part of the montmorillonite sample consisted of single plates. In the case of Laponite, rheological and turbidity measurements suggest that below 2% concentration Laponite platelets separate completely; i.e., they are fully dispersed.[50,51]

Laponite is a synthetic counterpart of natural hectorite clay with a layered structure. The layer is composed of two SiO_4 tetrahedral sheets and one MgO_6 octahedral sheet arranged in a TOT sandwich (T = SiO_4 tetrahedral sheet and O = MgO_6 octahedral sheet). The Mg^{2+} ions in the octahedra are partially substituted

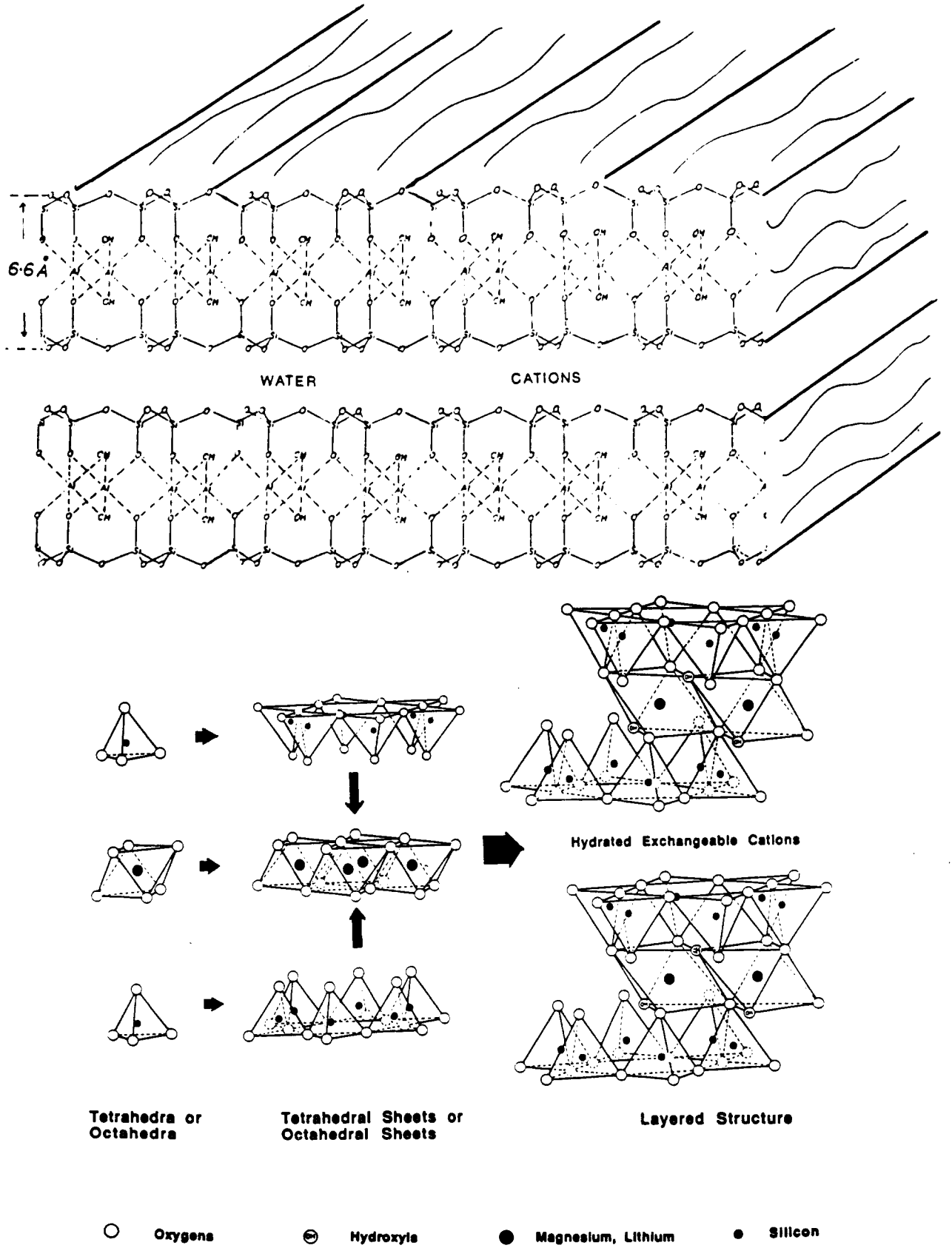

Figure 5. Diagramatic representation of a clay surface and structures.

by Li^+ ions, which provides the source of negative charge of the sheet. The negative charge produced by the substitution is compensated by Na^+ cations located in the interlayer space. The interlayer space can also accept water molecules and, as a consequence, is expanded to an extent, depending on the actual conditions of hydration. In an aqueous solution, laponite layers may separate completely and are present in the form of individual layers. On drying, the layers aggregate together and form particles with three or four layers in a stack.[51] The actual structure of Na^+–laponite may not be regular and may form a so-called "house of

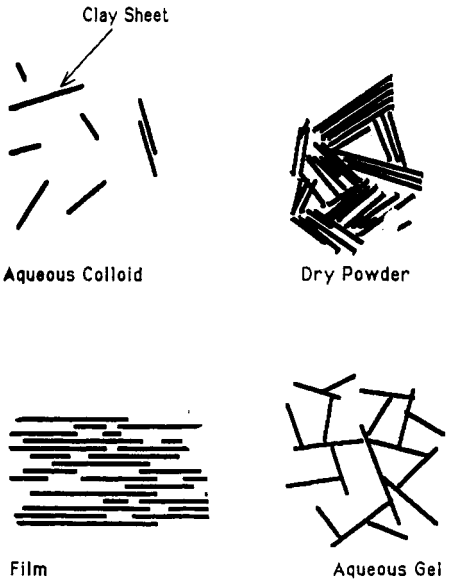

Figure 6. Structure of laponite colloids.

cards" structure, owing to the ease of delamination. The surface of a dried laponite particle is built up with the outer surface of the stack involving siloxane bonds and a lateral surface of the layers which include broken and terminated Si–O and Mg–O and/or Li–O bonds as well as an interlayer surface partially covered by the Na^+ cations. The hydrated form of laponite exhibits surfaces covered by water. Examples of the above clay and clay colloid structures are given in Figure 6.

VIII. Optical Measurements

The most widely used method of observing photochemical or radiolytic events on surfaces is UV–visible reflectance spectroscopy. In some instances conventional product analysis has been used. In transmission spectroscopy the intensity of the absorption bands are related to the concentration of the species via Beers Law. Intensity of emission is directly related to species concentration both in transmission and reflectance spectroscopy. The accepted theory describing the reflectance of finely divided opaque materials is that due to Kubelka-Munk. The theory was developed on the basis of the concept of absorption and scattering of light by the material[52,53] and can be represented by the equation

$$\frac{k}{s} = \frac{(1 - R_\infty)^2}{2R_\infty} \equiv F(R_\infty) \qquad (1)$$

where R_∞ is the reflectance of the sample and k and s are the absorption and scattering coefficients of the sample, respectively. In order to simulate the absorption spectrum of the sample quantitatively, the Kubelka-Munk function, $F(R_\infty)$, is essential. However, if the data only need to be treated qualitatively, other functions such as R_∞, $\log R_\infty$, $1/R_\infty$, $1 - R_\infty$ and $-\log R_\infty$ may be used instead because the maxima of these functions correspond to the maximum in $F(R_\infty)$.[54-56] Most reflectance data are presented in the form of $1 - R_T$ where R_T is the relative reflectance defined by the ratio of the reflectance of the sample to the reflectance of the background. In instances where the data needs to be treated quantitatively, the $F(R_\infty)$ is used. This function is calculated by using MgO as a standard.[57] In some instances infractive index matching may be used, as with SiO_2 and C_6H_{12}. The slurry is reasonably transparent and transmission spectroscopy can be used.

For the most part emission spectroscopy is not affected by the above factors.

IX. Treatment of Kinetic Data

In fluid solution, the rapid diffusive movement of the solvent and solute molecules lends itself to simple averaged disruptions of solute environment and of kinetic events. Single rate constants to describe processes are common in fluid solution. In solid solutions, i.e. polymer films or solid surfaces, such simple considerations are not common. More complex situations arise such as a variety of adsorption sites for the solute, which control its rate of reaction, the possibility of partial dimensionality exists.

The heterogeneous nature of the absorption sites and hence the heterogeneous nature of the solute environment has been considered by Albery et al.[58] and Scott.[59] The crucial point made is that an observed heterogeneity of a system can be approximated by a Gaussian distribution. Since an observed rate constant is a consequence of the free energy of a system, the distribution in the natural logarithm of observed rate constants is described by a Gaussian distribution; the distribution can be characterized through a mean rate constant, k, and a distribution parameter, γ. The dispersion in the first-order rate constants for $-\infty \leq x \leq \infty$ then becomes

$$\ln (k) = \ln (\bar{k}) + \gamma^x \qquad (2)$$

The observed decay profile is composed of the summation of the contributions from each microscopic species. Integration over the distribution, $\exp(-x^2)$, yields the following equation when the fluorescence intensity is proportional to the probe's excited-state concentration:

$$\frac{I(t)}{I(0)} = \frac{\int_{-\infty}^{\infty} \exp(-x^2) \exp[-\bar{k}t \exp(\gamma x)]\, dx}{\int_{-\infty}^{\infty} \exp(-x^2)\, d\chi} \qquad (3)$$

where

$$\int_{-\infty}^{\infty} \exp(-x^2)\, dx = \pi^{1/2}$$

and x is the integration range. After transformation of the variable, $x = \ln (\lambda)$ for $x < 0$ and $x = -\ln (\lambda)$ for > 0, the integration of the numerator of eq 3 can be carried out using the extended Simpson's rule; division of this integration by the denominator yields eq 4.

$$\frac{I(t)}{I(0)} = \frac{1}{\pi^{1/2}} \int_0 g(\lambda)\, d\lambda$$

$$g(\lambda) = \lambda^{-1} \exp[-[\ln (\lambda)]^2][\exp(-\bar{k}t\lambda^{\gamma}) + \exp(-\bar{k}t\lambda^{-\gamma})]$$

$$\frac{I(t)}{I(0)} = \frac{0.2}{3\pi^{1/2}}[2[g(0.1) + g(0.3) + g(0.5) + g(0.7) + g(0.9) + g(0.2) + g(0.4) + g(0.6) + g(0.8) + \exp(-\bar{k}t)]] \qquad (4)$$

Whereas the observed decay profile no longer is characterized by a single decay rate, the steady-state fluorescence intensity becomes dependent on both γ_{obs} and k_{obs}. The typical Stern–Volmer plot for homogeneous solution is no longer represented by eq 5, but

$$\frac{I_0}{I} = 1 + \frac{k_q}{k_0}[Q] \tag{5}$$

rather, by eq 6; see derivation 1, where k_q is the bimolecular quenching rate constant, k_0 is the mean probe's excited-state unimolecular decay rate constant, k_{obs} is the mean observed decay rate constant, γ_0 is the distribution parameter of the Gaussian for the unimolecular decay, and γ_{obs} is the distribution parameter for the observed unimolecular decay rate.

Derivation 1. Steady-state fluorescence intensity is defined as the integration of the fluorescence decay function $I(t)$.

$$I = \int_{-\infty}^{0} I(-t')\, dt'$$

$I(-t')$ is defined in the Gaussian distribution model through eq 3; note that the time transformation of $t = -t'$ has been made for convenience.

$$I = \int_0^\infty \left[\frac{1}{\pi^{1/2}} \int_{-\infty}^{\infty} \exp(-x^2) \exp[-\bar{k}t \exp(\gamma x)]\, dx \right] dt$$

Since these mathematical functions are continuous and can be differentiated, we can change the order of integration to

$$I = \frac{1}{\pi^{1/2}} \int_{-\infty}^{\infty} \exp(-x^2) \int_0^\infty \exp[-\bar{k}t \exp(\gamma x)]\, dt\, dx$$

The first absolute integration over t can be performed exactly to yield

$$I = \frac{1}{\pi^{1/2}} \int_{-\infty}^{\infty} \frac{1}{\bar{k}} \exp(-x^2 - \gamma x)\, dx$$

The second absolute integration over x can be converted to a Gaussian error function through the transformation of $z = x + (\gamma/2)$. Integration yields

$$I = \frac{1}{\bar{k}} \exp\left(\frac{\gamma^2}{4}\right)$$

Therefore, the final steady-state fluorescence expression becomes

$$\frac{I_0}{I} = \exp\left[\frac{(\gamma_0)^2 - (\gamma_{obs})^2}{4}\right] \frac{\bar{k}_{obs}}{\bar{k}_0} \tag{6}$$

The above treatment works well for colloids,[58] polyelectrolytes,[60] and Al_2O_3 and accurately describes photophysical events on SiO_2.[61,62]

Both reactants may be located on the solid surface, reaction then ensuing as both diffuse together on the surface. Alternatively one reactant may be located on the surface while the second reactant bombards the surface (and also the surface-bound reactant), from the gas phase above the solid.

The expression for the bimolecular rate constant for a Langmuir–Rideal type quenching scheme both for a smooth surface is eq 7, and for a porous solid in the Knudsen regime, where the pore diameter is much less than the gas-phase mean free path, the expression is as in eq 8.[63]

$$\frac{d[probe^*]}{dt} = \frac{1}{4} \frac{\alpha(\nu)\, \sigma_{probe}}{kT} P_q [probe^*] + \frac{[probe^*]}{\tau_0} \tag{7}$$

$$-\frac{d[probe^*]}{dt} = \frac{4}{6} \frac{\pi \alpha r_{ab} g R p(\nu)}{kT} P_q [probe^*] + \frac{[probe^*]}{\tau_0} \tag{8}$$

where

$$(\nu) = \left(\frac{8kT}{\pi m_w}\right)^{1/2}$$

α is the efficiency of the bombardment reaction, α_{probe} is the cross-section area of the probe, r_{ab} is the interaction radius for the reactants, g is a geometric factor ($g > 0$), R_p is the pore radius, τ_0 is the lifetime of the probe in the absence of quencher, P_q is the bulk gaseous quenching pressure, m_w is the molecular mass in kilogram per molecule of the gas, T is the absolute temperature, and k is the Boltzmann constant. Converting pressures to concentration units through the ideal gas law and defining the mean velocity (ν) we obtain eqs 9 and 10, where R is the ideal gas constant, from eq 7 and 8, respectively. Equations 9 and 10 show

$$k_q = R\sigma\alpha(2\pi m_w k)^{-1/2} T^{1/2} \tag{9}$$

$$k_q = \frac{4}{3} R R_p r_{ab} \alpha \left(\frac{2\pi}{m_w k}\right)^{1/2} T^{1/2} \tag{10}$$

that a gas-phase bombardment quenching mechanism would predict that the quenching efficiency should increase with the square root of temperature.

The porous nature of many solids, an essential property for providing a large surface area for adsorption, can lead to dimensionability problems which are usually discussed in terms of fractals.[64–68] For example the survival probability (B^*) of an excited donor surrounded by acceptors is given by

$$(B^*) = e^{\gamma[(t/\tau)(\bar{d}/6)+(t/\tau)]}$$

where $\bar{d}$ is the fractal dimension of the surface containing the donor and the acceptor, τ is the fluorescence lifetime, t is time, and γ is an adjustable parameter which contains the concentration of the acceptor.[68] The fitting of the data to the equation gives the fractal dimension $\bar{d}$. For the donor rhodamine B and the acceptor malachite given, in porous Vycor glass, the data are fitted with $5 = 6$ and $\bar{d} = 1.74$.[65]

A criticism of the above treatment is that experimental data can be fitted well by many different mathematical forms. Hence, often the tendency is to select a model, usually without experimental backing and discuss the data completely in terms of the suggested model.

Recent publications[63b,c] consider the mean free path to be all important in gas–solid reactions and indicate that the diffusion limited Smoluchowski equation does not describe kinetic events on these systems.

X. Photophysical Photochemical Studies

There have been a number of photophysical and photochemical studies of molecules adsorbed in SiO_2,

γ-Al_2O_3, and zeolites. Several excellent reviews are quoted.[69-76] The essence of the studies shows that (a) molecules diffuse slowly on the surfaces, (b) the surfaces are polar, (c) geometrical constraints, e.g. pore size, can affect second-order reactions in these systems, and (d) in some instances an active site of a reactant, e.g. amino group, becomes inactive on complexation with the surface.

For the most part the resulting photochemistry on surfaces is reminiscent of the reactions in polar homogeneous solution or micellar systems. The net outcome of the surface reactions is controlled by the surface features a to d given above.

Photophysical studies, as given in the reviews quoted, give valuable information on the nature of the solid surface. These studies complement conventional surface techniques such as heats of adsorption, infrared, and NMR spectroscopy and ESCA studies.

XI. Radiation and Photochemistry

A strict comparison of the action of high- and low-energy radiation on solids is governed by the following facts: (1) The high energy irradiation of SiO_2, γ-Al_2O_3, zeolites, and similar materials with adsorbed chromophores produces very low yields of excited states. By contrast low-energy photoexcitation of these systems produces significant yields of excited states (quantum yields ϕ, approaching unity). (2) High-energy irradiation (radiolysis) produces a low degree of damage into the lattice structure of the solids. This damage can act as a trap for subsequent chemistry.[2,77-79] Such effects are rare in photochemistry. (3) Ionic products and free radicals which are derived from the ions, are produced on radiolysis of solids with absorbates. In some instances ionic products are observed also in these systems with low energy excitation. To simplify the comparison of the chemical effects of the two types of radiation, the review is mainly confined to the ionic effects of the radiation.

A. Radiolysis of SiO_2

The action of high-energy radiation on solids is of importance in the design of materials for use in the nuclear industry. To this end there are numerous reports of the action of γ-rays or reactor radiation (neutrons) on solid materials. The concensus of opinion is that large irradiation doses (megarads, 1 rad ≡ 100 erg/gm) can lead to observable atom displacement on the crystal lattice. At lower doses (0.01 Mrad) organic molecules adsorbed on the solids are decomposed, the energy being absorbed initially by the solid and then being transferred to the adsorbate.[80,81] If the irradiations are carried out at 77 K, then reactive intermediates can be trapped, and they have been investigated by EPR and UV-visible spectroscopy. It is useful to list various findings:

The radical anions of various adsorbates are formed; these include tetracyanoethylene,[82] biphenyl,[83] CO_2,[84] and SO_2;[84] free radical traps e.g. galvinoxyl are bleached on electron reduction.[83] The radical cations of low ionization potential adsorbents e.g. tetramethyl-*p*-phenylenediamine are formed.[82]

Methyl radicals are formed with methyl halides,[83,86] and these convert to methane at 278 K.[85] Aliphatic hydrocarbons,[80,81] ethanol,[87] azoethane,[88] and isopropylbenzene[89] are decomposed when irradiated on SiO_2 or added subsequent to irradiation. The reactive species can be trapped on the silica and then react on subsequent addition of organic molecules. Addition of a mixture of isopropylbenzene and tetracyanoethylene to γ-irradiated silica produces the radical anion of the tetracyanoethylene and benzene. The yield of the products are large, *G* values of 4.6 being reported.[89] (*G* value ≡ molecules changed/100 eV of energy adsorbed.) The trapped methyl radicals readily react with O_2 on the solid surface at 77 K, the product being peroxy radicals.[86]

Some controversy exists on whether γ-irradiation of Vycor and SiO_2 alone at 77 K gives rise to trapped H atoms; positive[91,92] and negative reports exist.[85,86,90] It is interesting to note that the γ-radiolysis of Vycor with C_2D_4 is not the source of the H atoms as no D atoms are formed.[86] γ-Radiolysis of Vycor with the adsorbed H_2O, C_2H_4 does give H atoms and 3-methylpentane does produce H atoms.[90] The same work also reports D atoms from D_2O and CD_4. It should be noted that for the most part the SiO_2 is heated under vacuum for 24 h which removes a large part of the surface silanol group (~50%).[92] Some of the earlier work did not clearly state that the preparation of SiO_2 was carried out under such rigorous conditions. The status of the SiO_2 surface, in particular the OH content, is important since reactions such as $e^- + \equiv SiOH \rightarrow \equiv SiO^- + H$ can occur.

Irradiation of SiO_2 gives rise to color centers that absorb in the ultra violet.[93-97] The color centers are called E′ centers which are associated with trapped electrons. Visible color centers are associated with hole trapping on impurities such as Al. The conversion of isopropylbenzene to benzene[89] is associated with the disappearance of the E′ centers. These centers have also been termed acid centers.[98] It is suggested[89] that the chemistry results from a trapping of the free charge carriers produced on irradiation of SiO_2. The trapping efficiency of the organic adsorbate on the surface is comparable to that of the defects in the SiO_2 matrix. It is pertinent to note that visible color centers on Si/Al catalysts also catalyze chemical reactions.[99]

Similar effects, i.e. creation of E'_1 centers (oxygen vacancy), are produced by two photoirradiations (6.4 eV photons) of amorphous SiO_2.[100,101] The latter studies are a direct link between photochemistry and radiation chemistry.

There are also reports of similar experiments in porous Vycor glass.[86,102] The results parallel those seen with SiO_2, in some instances the trapped radical ions are more stable in the Vycor system. Color centers also develop in irradiated Vycor due to electrons trapped on the residual (up to 3%) boron in the glass.

B. γ-Al_2O_3 and Silica-Alumina Gels

Silica-alumina gels are favored industrial cracking catalysts, and to this end more work has been done on these solid systems rather than on γ-Al_2O_3 itself. In contrast to SiO_2, high-energy irradiation of γ-Al_2O_3 or Si-Al gels give rise to trapped species which exhibit visible coloration. Several studies[103-105] indicate that the coloration is due to interstitial Al. EPR studies give complex spectra that indicate a positive hole

trapped on a bridging oxygen atoms bonded to a substitutional Al atom, and positive hole[106] trapped on nonbridging oxygen. Many organic molecules but in particular isopropylbenzene (IPB) bleach the visible color, the product in the case of IPB being benzene. In catalytic work this particular chemical reaction is diagnostic for radical cation formation. The color center is bleached by several molecules e.g. H_2, but not by O_2, and the ability of the irradiated SiAl gel to form benzene from IPB decreases. No signal due to trapped electrons is observed, although they must be present. Several scavengers, e.g. H_2, C_2H_4, NH_3, and H_2S, reduce the yield of color centers and the EPR signals. It is possible to correlate the ionization potentials of the scavengers and their ability to remove the color center. This approach provides an estimate[104] of the effective electron affinity of the positive hole as between 9.8 and 12.1 eV. Electron traps, O_2, N_2O and CO_2, trap electrons produced during the irradiation and enhance the color and positive hole signal. In the case of CO_2 the anion CO_2^- is observed.

The studies on the radiolysis of SiO_2, porous Vycor, γ-Al_2O_3, and Si–Al gels or catalysts suggest that the prime action of the radiation on these oxides is the formation of positive holes and electrons. In some instances the ionic species are trapped on the pure oxides at defects, which may or may not be the result of the irradiation. Interstitial impurities, e.g. Al or boron, also trap the ionic species. At low temperatures (77 K) these species can last for days. Addition of adsorbates either prior to, or post irradiation react with the ionic species forming cations or anions characteristic of the absorbate. Subsequent chemistry is a direct result of the initial ionic species. The subsequent chemistry i.e. ion neutralization does not result in significant yield of absorbate excited states. This is consistent with experience in polar liquids where ion chemistry is the main result of radiolysis, and apparently this result also carries over to polar solids. From the concentration dependence of the adsorbent scavenging of the color centers, it is estimated that the radiation induced charge can move 50 Å, from its initial site of creation to the site of the adsorbate.

C. Zeolites

The prior Al–Si solid oxides are amorphous in character. Selected synthesis can result in the formation of ordered Si–Al–O compounds or zeolites, which were described earlier. Irradiation of various zeolites leads to the formation of electrons which are trapped in selected Na^+ clusters in the zeolite structure. This leads to colored zeolites and the colors of some zeolites are stable in vacuum.[107] Similar species are observed when zeolites imbibe sodium vapor.[108,109] In the latter case the Na metal ionizes, producing electrons which are trapped by sodium cations. The exact structures of these e^- sodium cation complexes are determined by EPR, and structures such as Na_4^{3+}, Na_3^{2+}, K_3^{2+}, etc. (i.e. $Na^{(n-1)+}$ with n up to 4, and n = 3, 4 and for K^{n-1} have been reported.[109–124] In sodium X and sodium Y zeolites two types of EPR signals due to the trapped electron and to the trapped positive hole are observed[108] on γ-irradiation. O_2 removes the trapped electron signal but only broadens the hole signal located on the oxygen lattice. Removal of O_2 regenerates the hole signal but not that due to the trapped electron. A pink color is observed which is associated with the trapped electrons. These details will be discussed later in the photochemistry of zeolites.

Chemical evidence of the trapped electron is also forthcoming[125] when N_2O removes the color centers or EPR signal and produces N_2

$$N_2O + e^- \rightarrow N_2 + O^-$$

The N_2 yield is used as a monitor of the reaction of e^- with other electron scavengers SF_6 CCl_4, etc. via competition kinetics. Water adsorbed on zeolite, 13x gives rise to H_2 on γ-irradiation.[126]

XII. Absorption Spectrum of Trapped Electrons

The electrons trapped in various Na^+ clusters in zeolites give rise to different absorption spectra. A recent publication[124] has calculated the spectrum of trapped e^- in sodalite. The Hamiltonian used is for an electron moving in an electrostatic field created by the ions of the zeolite framework. Various cluster arrangements are considered and compared with available absorption spectra for Na atoms in sodalite.

A. Photochemistry in SiO_2

1. Photophysical Studies

References 127 to 143 contain several studies related to photophysics of molecules adsorbed on SiO_2, and how the studies reflect on the nature of the SiO_2 surface. The approach is to place a "probe" molecule on the surface where its photophysical properties comment on the surface. The probe molecule is usually an arene such as pyrene which is adsorbed to the surface at silanol groups, which may be isolated, vicinal, or geminal. EPR and emission studies indicate that the molecules experience some mobility, both rotational and translational, on the surface. The degree of mobility often affects the final outcome of a reaction in the condensed state. Photophysics of acenaphthylene in solution gives rise to the cis and trans dimer, the excited singlet giving the former with the triplet state giving both isomers. The yield of cis with respect to the trans isomer increases with increasing surface coverage of the SiO_2 by the acenaphthylene. These data are indicative of a nonuniform coverage of the surface by the guest molecule, thus enhancing singlet-state interaction which gives the cis isomer. Studies of the enhancement of the triplet yield by energy transfer from excited rose benegal, and triplet quenching by ferrocene, are interpreted in terms of a movement of the triplet over 300 Å in 2 μs, while the excited singlet only moves 2 Å during the singlet lifetime. Long-lived species such as benzyl radicals produced in the photolysis of various benzyl derivations on SiO_2 are not troubled by the lack of mobility on the oxide surface, and dimerization takes place readily. Coadsorbates, e.g. long-chain alcohgols, tend to increase the mobility of adsorbed species, the effects showing up in both the photophysics and photochemistry. However, coadsorbates have little effect on reactions of long-lived species, such as benzyl radicals.

The photophysics of adsorbed molecules may also exhibit pronounced effects due to constraints placed on the molecules at the surface. The molecule 9,9′-

bianthyl (BA) exhibits a charge-transfer fluorescence in polar solvents and an anthracene-like fluorescence in frozen solvents at 77 K. However, when adsorbed on porous glass only the charge-transfer fluorescence is observed in all cases, even at 77 K. This indicates the ability of the molecule to adjust its geometry on the SiO_2 surface. Similar photophysical behavior is exhibited by binaphthyl,[137] which in fluid solution exhibits a broad emission spectrum which is red-shifted with respect to that seen in frozen solution. The emission in frozen medium is structured and is typical of the emission observed for excited naphthalene. The ability of the two naphthalene groups to rotate into conjugation is important in order to see the red-shifted broad emission. However, binaphthyl adsorbed on SiO_2 gives identical emission spectra at room temperature and at 77 K, indicating rapid rotation of the molecule in the solid even at low temperatures. An alternative conclusion is that the geometry of the adsorbed BA is that of the relaxed configuration.

There is substantial evidence that some of the molecules are adsorbed on the SiO_2 surface in zones or regions of relatively high local concentration. With pyrene, a ground-state dimer complex is postulated.[130] This species manifests itself by rapid or even immediate excimer formation on excitation and by an absorption band at 375 nm, which is observed in crystalline pyrene, on some surfaces, but not in solutions of pyrene. This behavior is also exhibited by naphthalene and also appears in the photochemistry of acenaphthylene. Coadsorption of long-chain alcohols to the SiO_2 surface disperses the pyrene aggregates, and excimer formation is then observed to grow in over nanoseconds following the excitation pulse. The growth of the excimer is due to limited movement of excited pyrene (Py*) and pyrene on the surface. Coadsorption of quenching molecules for excited pyrene, e.g. 2-bromonaphthalene and 2-iodonaphthalene, leads to a quenching of the pyrene emission. The mechanism is assumed to occur via a complex of Py* and the quencher Q. In cyclohexane the rate constant of dissociation of the complex, k_{dis}, is much larger than the complex radiative rate constant, k_r, $k_{dis}/k_r \gg 1$. However, on SiO_2 $k_r \geq k_{dis}$. The nature of the surface and, in particular, the part it plays in restricting lateral movement and cage escape of components from complexes is quite different on surfaces compared to solution. The above quenching studies can be used to illustrate intergranular migration of adsorbed molecules in SiO_2.

The probe, e.g. pyrene, may also be bound to the surface either chemically[141] or photochemically.[142] Any observed second-order reactions are then due to movement of the reactant to the immobilised pyrene.

2. Molecular Diffusion on SiO_2

Molecular diffusion is slow on most surfaces, due to the relatively strong forces of adhesion to the surface. Photophysical studies of triplet excited states may be used to measure surface diffusion, as the long lifetime of the triplet state extends the time window of the measurements from $\sim 10^{-7}$ to 1 s.

The triplet state of benzophenone is quenched by ferrocene at a rate of 7.3×10^{15} dm^2 mol^{-1} s^{-1} on 95 Å diameter porous silica and at 7.5×10^{15} dm^2 mol^{-1} s^{-1} on 255 Å diameter porous silica.[143-146] These numbers can be compared to those for the quenching of acenaphthylene triplet by ferrocene at 7.0×10^{15} dm^2 mol^{-1} s^{-1}. Other studies[128] have used triplet–triplet annihilation of acridine on SiO_2 and report a two-dimensional bimolecular rate constant of 8×10^{13} dm^2 mol^{-1} s^{-1}.[144] These authors also point out the importance of prior treatment of the SiO_2. Preheating at high temperatures ($T \sim 500$ °C) reduces the surface silanol content and markedly reduces the rate of adsorbate diffusion, no delayed fluorescence being observed for SiO_2 pretreated at high temperatures. A fractal approach to describe the kinetics has been tried in some studies.[145]

In some cases singlet quenching is possible as with excited pyrene quenched by halonaphthalenes.[128] In the solution phase the quenching efficiency increases some tenfold from 2-chloronaphthalene to 2-bromonaphthalene and continues for 2-iodonaphthalene; the rates are well below the diffusion controlled limit. However, on SiO_2 the rates are all similar and are indicative of an enhanced cage effect on the surface.

3. Nature of Surface OH

The adsorption sites in SiO_2 consist of silanol groups as single, geminal, or vicinal OH. Pyrene as a probe does not distinguish between the various regimes. However, aminopyrene (AP) readily distinguishes vicinal and geminal OH groupings on the SiO_2 surface.[147,148] AP on SiO_2 surfaces with isolated or vicinal OH groups produces a broad emission at $\lambda > 420$ nm, lifetime being 10 ns. AP on SiO_2 surfaces with geminal OH groups produces a structured emission on the 370–400-nm region with a lifetime of >100 ns, which is reminscent of pyrene. Studies in homogeneous solvents show that the pyrene-like emission arises from protonated AP where no conjugation exists between the NH_3^+ group and pyrene. The fluorescence data on SiO_2 geminal OH groups indicate that these entities donate a proton to the base AP and that the excited protonated species is stable over the lifetime of the excited state. Earlier work with aniline adsorbed on SiO_2 surface suggests[149a] that geminal OH groups adsorb water and act as proton donors. The aminopyrene acts as a sensitive monitor of the surface OH groupings.

Energy transfer between arene adsorbates on SiO_2 (low-temperature form) is very efficient and suggests that the adsorbates are adsorbed at small surface domains of silanol groups.[149b] Heating the silica above 450 °C removes the silanol groups, and all of the domains. Conventional energy transfer between randomly adsorbed arenes is then observed.

4. Free-Radical Reactions

Several studies have shown a marked cage effect of the solid surface on photophysical reactions.[128] Selected free-radical reactions also exhibit such phenomena, in SiO_2 and porous glass.[150-153] The basic concept behind these probing studies is the photolysis of a A–B system to give two fragments A and B the reactions of which reflect on their surroundings or containment. A favored molecule is dibenzyl ketone DBK, the photochemistry of which is shown in Scheme II. The extent of the cage effect is reflected in the relative yield of the products A–B, A–A, and B–B. The cage effect can be close to

Scheme II

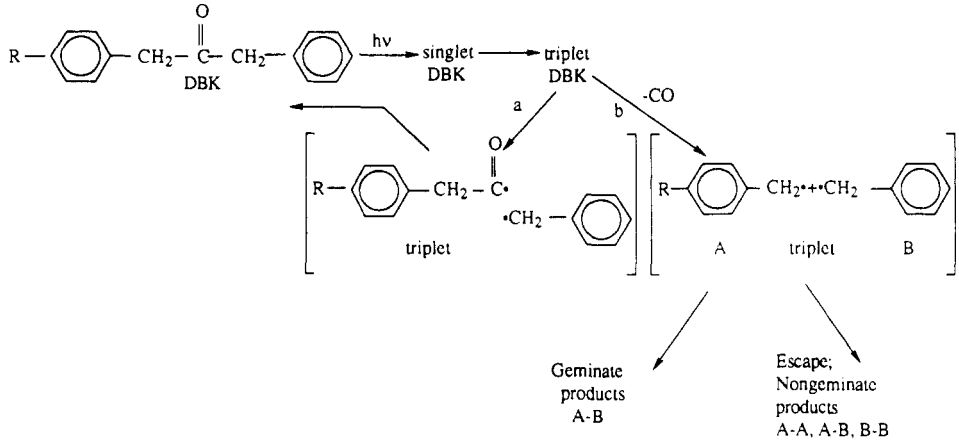

zero in homogeneous solvents such as benzene and 2-propanol and rise to 53% for porous silica.

5. Ionic Processes on Silica and Porous Vycor

Several materials illustrate photoionization in SiO_2 or porous Vycor. The list includes triphenylamine,[154,155] benzene,[155] and polyenes.[156,157] Excited ruthenium trisbipyridine disproportionates on porous Vycor to ruthenium(III) and ruthenium(I). In some cases an electron acceptor has to be present to prevent the return of the electron to the parent cation. In all instances the processes are claimed to be two photon in nature. The subsequent decay of the ions on the surfaces have fast (10^{-8} s) and slow components (seconds), and may be described by geminate ion neutralization or via electron tunneling. This will be discussed later under γ-Al_2O_3.

6. γ-Al_2O_3

Photophysical studies, similar to those on SiO_2, have also been carried out on γ-Al_2O_3, and to a large extent the data are similar to those obtained with SiO_2 systems.[157,158] A major difference exists, however, as charge-transfer complexes of many arenes are formed on γ-Al_2O_3, due to adsorption at Lewis acids sites. In some instances complete ionization takes place to form radical cations of the adsorbate. Increasing the preactivation temperature of γ-Al_2O_3 increases the number of Lewis acid sites. Electron donor–acceptor complexes (EDA) of several arenes, naphthalene, phenanthrene, and biphenyl are formed with the Lewis acid sites.[159-174] The EDA complexes are characterized by new unstructured fluorescence bands located at wavelengths shifted to the red of the spectra of the physically adsorbed species.

Both steady-state and time-resolved studies of γ-Al_2O_3, with pyrene, 1-pyrenecarboxaldehyde, and 1-aminopyrene indicate that there are a variety of adsorption sites on alumina for polyaromatic compounds.[175-177] Alumina, pretreated at low temperatures, tends to have a high concentration of surface OH which H bond with adsorbed molecules. On the other hand alumina pretreated at high temperatures has surface Lewis acid sites which produce cation radicals of adsorbates. Pretreatment at intermediate temperatures produces surface sites which form charge-transfer complexes with adsorbates. The Gaussian distribution kinetic model is used to describe the decay of the singlet excited state of pyrene ($^1P^*$). The average decay rate constants of $^1P^*$ range from 6.85×10^6 to 1.21×10^7 s^{-1} for pretreatment temperatures from 140 to 750 °C. The reaction of $^1P^*$ with coadsorbed quenchers such as nitrobenzene and nitromethane changes from dynamic to static in nature when the pretreatment temperature is increased. At high pretreatment temperatures, a large number of Lewis acid sites induces formation of cation radicals of the probes, which are characterized by their characteristic cation absorption spectra, $\lambda_{max} = 450$ nm. The cation radicals of pyrene and aminopyrene do not luminesce on excitation, but that of pyrenecarboxaldehyde exhibits an emission at 520 nm. The studies are the first report of a quantitative kinetic description (Gaussian in k) of photochemical events at active sites of alumina.

As in the case of pyrene on SiO_2, O_2 efficiently quenches the fluorescent state of pyrene. The efficiency of the processes decreases with decreasing temperature over the range 70 to −10 °C, but increases with temperatures over the range −30 to −70 °C. This indicates that over the range +75 to −10 °C, where the oxygen adsorption is relatively small, the mechanism of the quenching process is a bombardment from the gas phase, but the mechanism switches to one involving adsorption on the surface to low temperatures when oxygen adsorption on the surface increases. The bimolecular quenching rate constants, k_q, were calculated to be 1.51×10^8, 1.47×10^8, 1.43×10^8, and 1.31×10^8 m^3 mol^{-1} s^{-1} at 75, 48, 23, and −10 °C, respectively. These numbers are in agreement with the results from the time-resolved studies, but they are ~3 times greater than the values found for quenching of $^1P^*$ on silica gel surfaces i.e., 5.12×10^7 m^3 mol^{-1} s^{-1}.[62] This also bears out the hypothesis that the mechanism for oxygen quenching on the alumina surfaces is via O_2 bombardment from the gas phase.

If the bombardment mechanism is operative at high temperatures, the quenching rate constant should be proportional to the frequency of surface collisions. The total collisional frequency per unit area, Z, is related to the absolute temperature by the following equation:[63]

$$Z = n(kT/2\pi m)^{1/2}$$

where n and m are the concentration and the mass of oxygen, respectively. The above equation predicts that the ratios of k_q at 23, 48, and 75 °C to k_q at −10 °C are

1.06, 1.10, and 1.15, which agrees with the measured value of this study, 1.09, 1.12, and 1.15. This indicates that oxygen quenching on alumina surfaces at higher temperatures takes place via an O_2 bombardment mechanism. The triplet state P^T and the cation radical P^+ of pyrene are produced on excitation of pyrene adsorbed on γ-alumina.[175] The characteristic absorption spectra of these two alumina-bound transients are similar to those in solution and exhibit absorption bands at 415 and 450 nm for the triplet and the cation, respectively. The triplet state decays exponentially with a lifetime of 5.1 ms, while the cation decays in a more complicated fashion which can be described by a Gaussian distribution of the logarithm of the rate constant at various adsorption sites. Movement of ferrocene to the triplet state on the surface quenches the triplet via energy transfer. The bimolecular quenching constants of pyrene triplet by ferrocene are 3.31×10^{11}, 2.63×10^{11}, and 2.20×10^{11} m^2 mol^{-1} s^{-1} for alumina at pretreatment temperatures of 130, 250, and 350 °C, respectively. Pretreatment of the alumina surface at high temperature decreases the number of surface hydroxyl groups. The physiadsorbed molecules at the OH are bound less strongly than those at the acidic sites formed at high pretreatment temperatures. Hydration of the surface by small amounts of coadsorbed water increases the number of surface hydroxyl groups and enhances the degree of dynamic quenching. The quenching of P^+ by ferrocene could involve the diffusion of both or either one of the reactants on the surface. To select which molecule diffuses in the reaction, use is made of the ferricenium cation. Ferricenium ion exhibits dynamic quenching of triplet pyrene in homogeneous solution with a quenching rate constant of 1.05×10^9 M^{-1} s^{-1}, a value which is close to that of a diffusion-controlled reaction. Ferrocene interacts strongly with the Lewis acid site via electron transfer forming ferricenium ions; the latter do not quench P^T. At $T_a = 450$ °C, a greater number of Lewis acid sites are produced so that the greater amounts of ferricenium ion are formed. A dynamic quenching interaction between the triplet of pyrene and absorbed ferricenium ion still could not be detected. These data show that ferricenium ion does not quench P^T under conditions where ferrocene quenches efficiently. Hence, quenching of P^T is the result of diffusion of ferrocene to P^T, which is immobile over the time range of the study.

Earlier work[144] reported that triplet acridine diffuses on SiO_2 surfaces but not on γ-Al_2O_3. The lack of diffusion of triplet pyrene on γ-Al_2O_3 is in agreement with this report.

Oxygen quenches the triplet state of pyrene on alumina surface with a bimolecular rate constant of 4.82×10^4 $Torr^{-1}$ s^{-1}, which is about 160 times slower than that of quenching of the singlet excited state of pyrene on the same surface (7.9×10^6 $Torr^{-1}$ s^{-1}).

In solution the relative rates of quenching of the singlet and the triplet of pyrene by oxygen is 9:1. The much larger ratio of 160-fold observed on alumina and the ratio of 30 on silica is primarily due to the lack of a cage effect on the solid surfaces compared to cage effects in solution. The singlet–oxygen reaction is diffusion controlled in solution while that of the triplet is 1/9 of diffusion controlled due to the spin selection exhibited by the reaction.[178] The solvent cage ensures that many collisions of the triplet and oxygen occur on one encounter of the two reactants. On a solid surface no cage exists and simple collision of the triplet and oxygen occurs. Since the reaction is not diffusion controlled, the rate is reduced, compared that for the quenching of excited pyrene singlet by oxygen. Coating the surface with liquid cyclohexane provides a solvent cage for the reaction, and the ratio of oxygen quenching of the singlet and triplet of 10:1 for silica and 12:1 for alumina which approaches that observed in solution.

The pyrene radical cation[176,179] and the radical cations of distyrylbenzenes[173] are formed on SiO_2 and γ-Al_2O_3 via two photon processes. The cations decays are nonlinear as illustrated in Figure 7. In the case of pyrene an initial fast decay is observed which decreases with time to get a small net permanent (days) yield of pyrene cation. Similar results occur with the styrylbenzenes but here the reaction is completely reversible in minutes. The kinetics are described by the relationship[180,181]

$$\frac{-d(c)}{dt} = kt^{-n}$$

The general kinetic behavior in the two systems is smilar and the decay of the radical cation is via neutralization by the negative component, i.e. the electron. The ion pair is considered to be geminate in nature, and the neutralization occurs by diffusion of the reactant pair[173] or via electron tunneling.[179]

The initial part of the pyrene cation decay can be fitted with a Gaussian function,[176] as indicated earlier Figure 8 shows the fit of the experiment data with the Gaussian calculation at various ferrocene concentrations.

$$\frac{c_t}{c_0} = \frac{\int_{-\infty}^{+\infty} \exp(-x^2) \exp[-\bar{k}t \exp(\gamma x)]\, dx}{\int_{-\infty}^{+\infty} \exp(-x^2)\, dx}$$

The reaction portrayed is

$$\underset{\text{cation}}{P^+} + \underset{\text{ferrocene}}{(Fe)_0} \rightarrow P^+ + \underset{\substack{\text{ferricinium}\\ \text{ion}}}{Fe^+}$$

The quenching rate for the above equation is 3.39×10^{11} m^2 mol^{-1} s^{-1} with γ-Al_2O_3 activated at 130 °C and is close to that measured for $(Fe)_0$ quenching of P^T. For reasons given earlier the ferrocene is the reactant that diffuses on the surface over the time scale of the reaction.

Photoinduced electron transfer have also been studied in SiO_2 and porous Vycor glass. With porous Vycor photoinduced e^- transfer between indium(III) and 1,4-dimethyloxybenzene (DMB), results in In(II) and DMB^+.[182] The glass retards the back-electron transfer by 4 orders of magnitude. In this system the indium-(III) is located on the glass while the DMB is in the pure water phase in the glass pores. Excited pyrene and diethyl aniline[183] exhibit no reactivity until a monolayer of the aniline is achieved on the solid surface. After this stage the reaction proceeds in the aniline layer, but unlike polar solution, no production of ions is observed. This is probably due to a rapid back-electron transfer of the pyrene anion and aniline cation

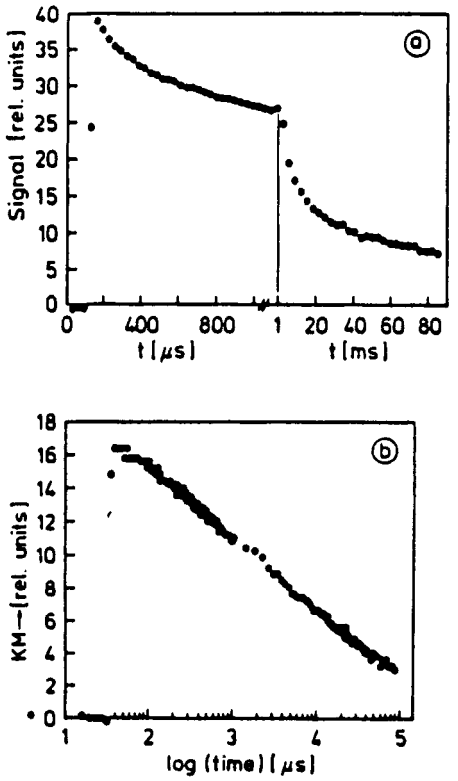

Figure 7. Decay of P^+ on γ-Al_2O_3.

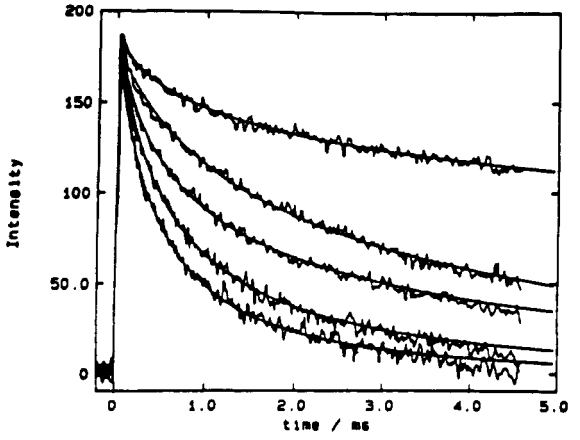

Figure 8. Decays of the cation radical of pyrene at various concentrations of adsorbed ferrocene (T_a = 130 °C) with the Gaussian distribution fit to data: 0, 2.15×10^{-7}, 4.30×10^{-7}, 6.46×10^{-7}, and 8.6×10^{-7} mol/g.

before the ions can diffuse apart on the surface. This is also noted for this reaction in viscous polar liquids.

As indicated, several mechanisms have been put forward to account for the nonlinear decay of cations on SiO_2 and γ-Al_2O_3. In general the description of the geminate process is similar in all systems, while rigorous quantitative differences are emphasized in each separate model. These differences could be due in part to (a) the different chemical systems used, (b) different solid surfaces in each study, and (c) different mode of producing the cation (laser pulse length, laser power, etc.).

The different excitations could produce a different distribution of geminate pairs, which fit one model more closely than another.

Further work is required in this area, and the point will be discussed later.

B. Zeolites

A considerable amount of photophysics and photochemistry has been carried out in various zeolites. For the most part the aim is to work on the inner space of the zeolite, this is usually achieved with zeolite X or Y while reactions occur on the surface of zeolite A due to its small pore size. The adsorbed alkali cations (Na^+, K^+, etc.) have a marked effect on the observed photoevents in zeolites. The exact location of these cations in the structure is important, an excellent description is given in ref 73.

For the most part imbibed organic molecules are located in the supercages. Pyrene,[76,184-186,189] anthracene,[187] and ruthenium trisbipyridine[188] (a few among many guest molecules) have been located in the supercages of zeolite X and Y, and all illustrate via their emission spectra and decay characteristics marked effects of coadsorbed solvent, nature of zeolite (X or Y), and nature of counter cation. Alkali cations, Li^+, Na^+, K^+, etc., have no effect on the photophysics of arenes in solution, while marked affects are observed in zeolite provided the zeolites is thoroughly dried.[73,186] A marked quenching of the excited singlet state is observed with an increase in the triplet yield due to enhanced intersystem crossing. The effect has been labeled a light atom effect[73] (in contrast to the customary heavy atom effect) since the lighter atom shows the effect more clearly and gives a greater interaction with the arene probe, in this case pyrene.

Typical steady-state fluorescence spectra (Figure 8) of pyrene in NaY at high and low loading under hydrated and dehydrated conditions are shown in Figure 9. Table II summarizes the results of the III/I ratio in different alkali-cation exchanged zeolite X and Y samples under fully hydrated and dehydrated conditions. The low value of the III/I indicates a very polar medium for pyrene in both zeolites. Increasing the pyrene concentration increases the III/I ratio as pyrenes are located closer together in the different zeolite cages. This also leads to excimer formation which is observed around 475 nm; however, coadsorption of water into the dehydrated sample decreases the dimer concentration. This is due to the strong interaction between the water and the zeolite framework which limits the space available for dimer formation (vide infra). Dimer formation occurs at much lower pyrene concentrations in zeolite Y (>5×10^{-6} mol/g) compared to zeolite Z (>2×10^{-5} mol/g). This is probably due to the subtle difference of the entry apertures between zeolites X and Y as the framework Si/Al ratio increases from zeolite X to zeolite Y (unit cell dimension decreases with increasing Si/Al ratio due to the different Si–O (1.62 Å) and Al–O (1.75 Å) bond length). Pyrene excimer is formed within 1 ns of excitation. This shows that little or no movement of the excited pyrene and ground-state pyrene is required to produce the excited dimer.

Coadsorbed solvents, alkanes, water etc. block the channels of the zeolites and hinder diffusion of gases such as O_2. Quenching effects of O_2 are thus reduced markedly or even eliminated by coadsorbed solvents to the extent that phosphorescence of arenes is readily observed in these systems. Such effects are not observed with zeolite A where arenes are adsorbed on the exterior surface of the zeolite.

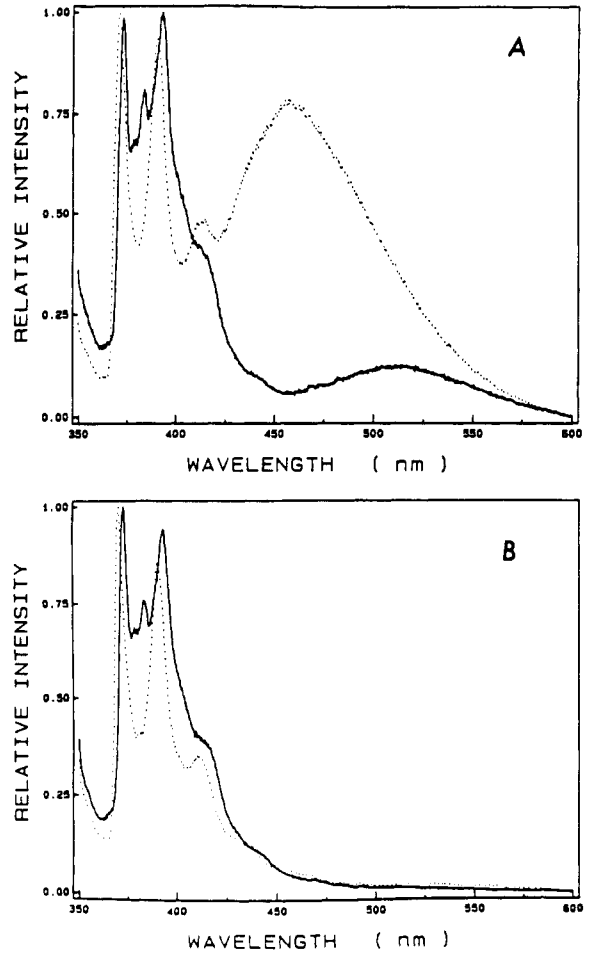

Figure 9. Steady-state pyrene emission in NaY: (A) 1.37×10^{-6} mol/g, and (B) 1.55×10^{-7} mol/g. The dotted line indicates dehydrated and vacuum. The solid line indicates hydrated and exposed to air.

Table II

zeolite X	hydrated	dehydrated	zeolite Y	hydrated	dehydrated
LiX	0.489	0.455	LiY	0.792	0.422
NaX	0.496	0.486	NaY	0.814	0.513
KX	0.374	0.328	KY	0.627	0.423

There are many studies of free radical reactions in zeolites. In particular, molecules of the type A–B are photolyzed to give products A–A, B–B, or A–B according to the cage effect.[70,71,73,74] The experiments are analogous to those discussed earlier in SiO_2, and again in the case of zeolites strong cage effects are observed on the product distribution in the reaction.

Reports of electron transfer in zeolites indicate a strong effect of the structure on charge stabilization. Irradiation of ruthenium trisbipyridine (Ru(II)) and methyl viologen (MV^{2+}) in zeolites produces reduced methyl viologen $MV^{\bullet+}$ which is blue, the color persisting for days. Similar effects are observed for the system in cellophane.[190] Charge-transfer complexes of methyl viologen and arenes are enhanced in the supercages of zeolites. Photolysis into the C–T band produces complete charge separation to give ion pairs which are stabilized nearly 10^6 fold compared to that observed in solution.[191,192]

Cu^{2+} or Tl^+ quenches P^S efficiently in zeolite X,[186] and the quenching mechanism is electron tunneling in nature. Exchanged Hg^{2+} or Pb^{2+} also readily quench singlet excited pyrene P^S in the supercage of NaX. Basically, the electron-tunneling model is an electron-transfer process as follows:

$$P^S + \text{cation}^{n+} \rightarrow \text{pyrene}^+ + \text{cation}^{(n+)-1} \quad (11)$$

The kinetics follow an electron-tunneling model via the equations below (eqs 12–14):

$$I = I_0 \exp(-k_d t) - A[\ln^3(\nu t) + h_1 \ln^2(\nu t) + h_2 \ln(\nu t) + h_3] \quad (12)$$

where A is a factor which depends linearly on the quencher concentration and k_d is the rate constant of the fluorescence decay in the absence of quencher. The h_1, h_2, and h_3 are coefficients related to derivatives of the Γ function, derived by Tachiya and Mozumber,[193] t is the time, and ν is the vibrational frequency in a square (or rectangular) potential well. For a first-order approximation, the rate of electron transfer in electron-tunneling model is similar to a free particle in a one-dimensional box as described in quantum mechanics. The square potential well is essentially the potential curve of P^S in our case. Fitting the time-resolved pyrene fluorescence (400 nm) of the cation exchanged zeolite X yields the parameters A, k_d, and ν. The electron transfer rate $k_{(r)}^{n-}$, in terms of the distance between the two species may be expressed in the following form:

$$A = \frac{[Q]}{(R_o/a)^3 C_o} \quad (13)$$

$$h_1 = -3\Gamma'(1) - 1.731\,646\,99$$

$$h_2 = 3\Gamma''(1) - 5.934\,335\,97 \quad (14)$$

$$h_3 = -\Gamma'''(1) - 5.448\,744\,5$$

$$k_{(r)} = \nu \exp(-r/a)\ \text{s}^{-1} \quad (15)$$

The equation requires a, which is the attenuation length of the wave function, and may be obtained from eq 13.

The nature of electron-tunneling kinetics, a very fast falloff in decay rate with distance, is well approximated by the static Perrin model. In other words, the initial rapid quenching at small r may be considered to be static, while the slow quenching at large r may be considered to be approximately that observed in the absence of quencher. Following this assumption, the Perrin model is applied to the cation quenching data to obtain C_o and R_o in eq 13. The R_o, which has the same meaning as the radius of the "active sphere" in the Perrin model, is the critical transfer distance for the electron-tunneling model; the C_o, as in the Perrin model, is the critical quencher concentration. In the Perrin static model, a plot of $\ln(I_o/I)$ vs [Q] should be linear and yield a slope of $1/C_o$. The R_o can be further determined by using the following equation:

$$R_o = (3 \times 10^{27}/(4\pi N C_o))^{1/3}\ \text{Å}$$

where N is Avogadro's constant. Table III summarizes the pyrene fluorescence quenching results of the exchange cations studied based on the electron-tunneling model.

Table III

exchange cation	dehydrated active radius (Å)	dehydrated ν ($\times 10^{-10}$)	dehydrated a (Å)	hydrated active radius (Å)	hydrated ν ($\times 10^{-10}$)	hydrated a (Å)
Tl^+	11.1 ± 1.0	0.07 ± 0.08	1.9 ± 0.6	16.0 ± 1.6	2.9 ± 0.9	1.2 ± 0.3
Cu^{2+}	15.1 ± 1.0	3.1 ± 1.7	1.4 ± 0.6	13.3 ± 3.3	0.5 ± 0.2	1.6 ± 1.2
Hg^{2+}	8.1 ± 2.2	5.9 ± 1.5	0.7 ± 0.6	7.9 ± 1.3	5.3 ± 2.1	0.6 ± 0.3
Pb^{2+}	8.7 ± 1.8	1.2 ± 0.5	0.8 ± 0.6	7.4 ± 2.9	2.5 ± 0.6	0.7 ± 0.8

Another study of interaction through space in zeolites is singlet–singlet energy transfer using P^S as an energy donor and perylene as an energy accepter. In a Förster-type interaction, the time dependence of the pyrene fluorescence can be expressed as in eq 16.

$$I = I_0 \exp(-k_d t\gamma - 2(-k_d t)^{1/2}) \quad (16)$$

where

$$\gamma = C_A/C_A^\circ \quad (17)$$

In eq 16, the I_0 denotes the initial pyrene fluorescence intensity (at time zero), k_d denotes the decay rate constant in the absence of quencher. By applying the nonlinear least-squares fitting routine to the time-resolved pyrene fluorescence (400 nm) with the form of eq 16, the γ values were extracted at different perylene concentrations. The critical accepter concentration (C_A°) was calculated by using eq 17, which further yields the critical transfer distance (R_0) via eq 18:

$$R_0 = [1500/(\pi^{3/2} N C_A^\circ)]^{1/3} \times 10^8 \text{ Å} \quad (18)$$

where N denotes Avogadro's constant and the unit of C_A° is in mol/L. The initial transfer distances calculated from the data are 38.9 ± 3.0 and 37.6 ± 1.4 Å for the hydrated and dehydrated, respectively. As expected these data in zeolite X indicate no effect of water on this type of reaction.

1. Photoionization

Photolysis of pyrene or anthracene in zeolite X or Y produces trapped electrons,[194] which are identical to those observed in pulse radiolysis of these zeolites in the absence of arene.[195] The trapped electrons are stable in X and Y at 77 K and also in Y at room temperature. EPR spectra show that the electron is trapped by Na^+ clusters, as Na_4^{3+}, Na_3^{2+}, and Na_2^+. Potassium also traps e^-, but Li^+ gives no evidence of an electron Li^+ species. The cation radical of pyrene or anthracene as well as the triplet state are also formed as shown in Figure 10. As the cation and e^- are produced equivalently, then the extinction coefficient of Na_4^{3+} is similar to that for P^+ and is indicative of an allowed transition in the spectrum. The mechanism of the photolysis is given in Scheme III, and photoionization occurs by one- and two-photon processes. Figure 10 shows the spectrum of Na_4^{3+} at 535 nm the spectra of the smaller clusters are red-shifted with respect to this spectrum.

The radiolytic and photoproduced e^- are identical in identical zeolites and under standard conditions. The radiolytic method has the advantage of producing e^- in the small cages of zeolite A, where no arene can be imbedded into the structure. The trapped electron spectra are quite stable, for days in the case of zeolite

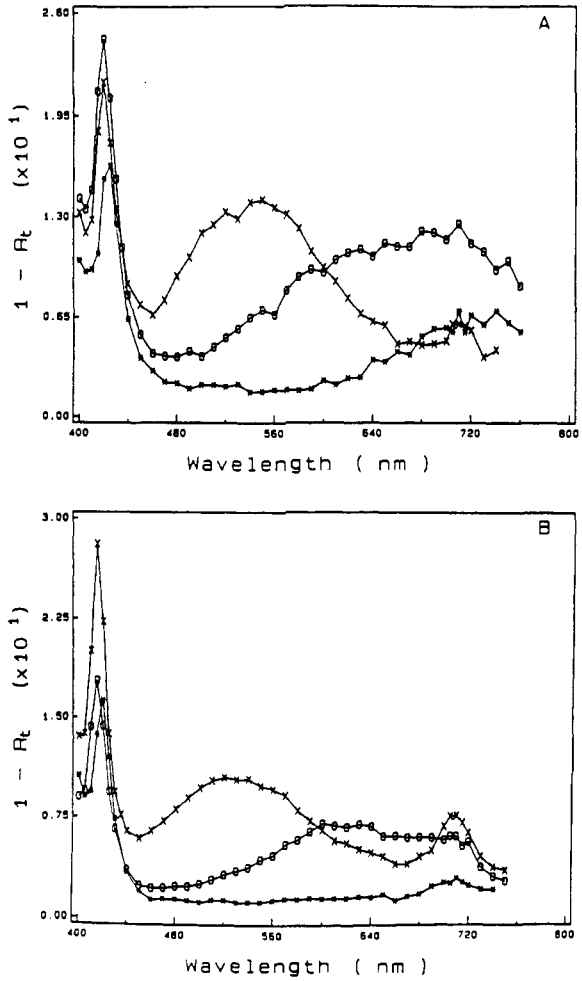

Figure 10. Diffuse reflectance spectra of dehydrated anthracene-impregnated alkali-metal-cation-exchanged zeolite immediately after the laser excitation: (A) zeolite X samples under vacuum (10^{-3} Torr), (B) zeolite Y samples under vacuum (10^{-3} Torr), (×) Na-exchanged zeolite, (○) Li-exchanged zeolite, and (*) K-exchanged zeolite.

Scheme III

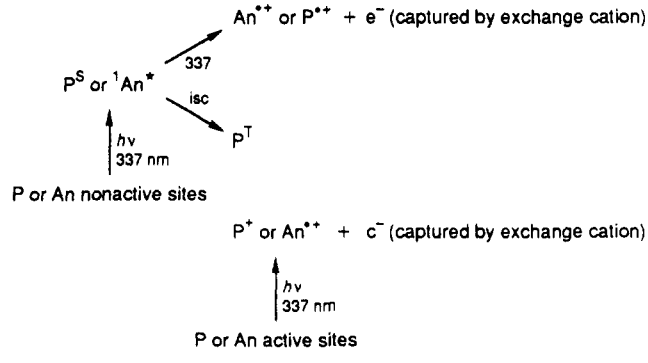

Y. In dry zeolites, oxygen increases the rate of decay by e^- transfer and forms O_2^-. However, the rate of decay depends on the zeolite due to the access of O_2 to the cage where e^- is trapped.

2. Semiconductor Formation

Semiconductors may be constructed inside the zeolite cages,[197-200] the rational being to form very small clusters. Semiconductors of small dimensions are found in several zeolites. A number of semiconductors such as CdS, CdSe, and PbS have been incorporated into zeolites such as sodalite, A, X, Y, chabazite, L, offerite,

and ZSM-5. The structures of the zeolites contain cages and with channels. Formation of semiconductors in these zeolite matrices, depends on factors such as location of the cations, migration of the cations, strength of the interactions between cations and guest molecules (H_2S in the case of CdS) and dimensions of cavities and channels. The most widely used zeolites for semiconductor synthesis are zeolites X, Y, and sodalite. All three zeolites contain a common β-cage, along with other cages such as α-cage and double-four-membered ring (D-4) in A and a supercage and a double-six-membered ring (D-6) in X and Y. Because of the smaller size of the D-4 and D-6 cages, it is commonly accepted that no CdS particles are located in the cages. However, for the bigger cages, both occupation of the supercage (α-cage in the case of zeolite A and supercage in the case of zeolites X and Y) and β-cages (sodalite cages) by CdS particles are proposed.[199,200]

The results of studies on the formation and photophysical properties of CdS in zeolites indicate that the CdS particles formed in zeolites X, Y, and A are located in the biggest cages of these zeolites. The evidence for this comes from the following experiments: (1) formation of CdS in zeolite sodalite;[199,197] (2) location and migration of Cd^{2+} cations in zeolite A, X, Y, and sodalite,[197] and (3) the formation of CdS in zeolite X in the presence of trace amount of Cu^{2+} cations. The commonly used procedure for preparation of CdS in sodalite, i.e. ion exchange of zeolites with Cd^{2+} cations followed by dehydration and inteaction with H_2S gas, leads to inefficient formation of CdS in its sodalite cages. In this case, only trace amounts of CdS could be obtained on the external surface of the sodalite, as shown by the very weak absorption spectrum of CdS.[198] This is expected from the difference between the entry aperture of the sodalite cage (2.1 Å for the biggest ring on the cage) and the size of the anions S^{2-} (3.5 Å in diameter).

Because of the presence of the β-cage and supercage in zeolites A, X, and Y, it seems reasonable to expect that the CdS particles are formed more easily in the supercages than in the β-cages. Studies on the location and migration of Cd^{2+} cations in zeolites A and X using an IR technique confirm this suggestion. The IR studies show a new absorption band around 932 cm^{-1} which has been shown to be due to the Cd^{2+} species present in the sodalite cages.[201] The absorption band may act as a probe providing information on whether or not the Cd^{2+} cations in the β-cage are involved in the process of CdS formation. Here two samples may be examined: a fully ion-exchanged zeolite X ($Cd_{36}X$) and a reverse-exchanged zeolite X ($Cd_{19}X$). The maintenance of the IR band in the sample CdS–$Cd_{36}X$ and the disappearance of the band in the sample CdS–$Cd_{19}X$ clearly demonstrated that in the former case, the Cd^{2+} cations in the small β-cage do not participate in CdS formation. In the latter case, the Cd^{2+} cations in the β-cage are the main source of Cd^{2+} for the CdS formation. Furthermore, similar adsorption and emission spectra are obtained for both samples, which also supports this conclusion. Even though the overall amounts of Cd^{2+} in both cases are different, due to migration of the Cd^{2+} cations from β-cage to supercage in the latter case, the amounts of Cd^{2+} used for CdS formation are the same.

Silver ions may replace Na^+ in zeolites and their luminescence used to comment on the zeolite structure.[202] Excitation of zeolite-bound Ag^+ in the presence of water leads to O_2 formation presumably by the following process

$$H_2O + (Ag^+)^* \rightarrow Ag + H_2O^+ \rightarrow O_2$$

If chloride ion is present then Cl_2 replaces the O_2.[203] The mechanism could be similar to that proposed for the Ag/AgCl colloid photolysis of water with reaction via H_2O^+ [204]

$$H_2O^+ + H_2O \rightarrow H_3O^+ + OH$$

$$OH + OH \rightarrow H_2O_2 \rightarrow O_2 + H_2O$$

$$OH + Cl^- \rightarrow Cl + OH^-$$

$$Cl + Cl \rightarrow Cl_2$$

C. Clays

For the most part the photochemistry on clays has been restricted to aqueous colloidal clay systems.[75,76] Colloidal clays only adsorb cationic material via exchange with the counter cation of the clay surface. The adsorbed organic cations tend to aggregate on the clay surface and can produce unique orientations at the clay surface.[205-209] Cationic surfactants can produce a layer of organic material at the clay surface, thus making the clay material dispersable in organic solvent. Further addition of surfactant produces a bilayer with next positive charge which now disperses in water. Photochemistry can be carried out in these layers.[207,208]

Several factors affect the photophysics and photochemistry on clays, the nature of adsorbed water[210] on the surface and the spacing of the clay layers.[211] A discussion of clays in the context of several different layered materials has recently been published.[212]

If clays are heated above 100 °C to drive off adsorbed water, then the dried clay readily adsorbs arenes from alkane solution.[213-215] Active sites such as Lewis acids are produced on the heated clay which undergoes electron transfer with adsorbed arenes, producing radical cations.[215] Ultraviolet irradiation of these dry systems produces further large yields of radical cations by photoinduced e^- transfer. Back-electron transfer is slow and the radical ions have lifetimes of several hours.[216,217] The formation of pyrene cation radicals is shown to be a single photon ionization process. This was achieved by varying the intensity of UV light and by irradiation in the presence of O_2 The mean lifetime of the pyrene cation radical created on the surface of Na^+–laponite ($t_{1/2}$) is 74 h. There is a distribution of electron-accepting sites on the surface which ionize the adsorbed pyrene molecules. Most of the active sites (82–86%) are located on the lateral surface, while others (14–18%) are located elsewhere in the regions that are unaffected by adsorbed water, polymetaphosphate, and basic molecules such as NH_3.

Several stable radical cations, pyrene, perylene, anthracene, and *N,N*-tetramethylphenylenediamine (TMPD) are produced thermally or photolytically on laponite clay. The photoproduced ions are stable for

hours under vacuum, but eventually recombine to reinstate the arene. The TMPD cation radical is produced mainly through a thermal channel which is unaffected by the presence of oxygen. The other cation radicals are also produced thermally, but the yields are greatly increased by exposure to UV light (300 nm) under vacuum. Oxygenated samples exposed to UV radiation produce cation radicals and unknown colored products. The luminescence of pyrene, perylene, and TMPD cation radicals on laponite are also observed.[215] Time-resolved pulsed-laser diffuse-reflectance studies show no trace of any trapped electron species within the 400–800-nm spectral range. The identification of the radical cation is via ERR, UV–visible, and infrared spectroscopy.[215]

1. Semiconductor Formation

Laponite,[219–221] porous Vycor glass,[220,222] and molecular sieves, faujasite X, and sodalite, have been used to prepare small particles of CdS with limited dimensions. Laponite limits one dimension of the CdS particles by the interplanar spacing of 11.5 Å. Porous Vycor glass limits two dimensions of the CdS particles to <40 Å (and a "quantum wire" is formed. Molecular sieves were used to limite the particle size to the size of the cavity; however, the particles constructed were larger than the cavity dimensions. The absorption onset and main emission wavelength increase with increasing Cd^{2+} concentration. The spectral properties of PdS are also reported. Methyl viologen and Cu^{2+} quench two different emission bands arising from CdS on laponite in solution. Methyl viologen quenches the high-energy emission, thought to arise from exciton recombination, while Cu^{2+} efficiently quenches a low-energy emission though to arise from S^{2-} deficiencies. Methyl viologen shows dynamic-type kinetics, while the static-type kinetics observed from Cu^{2+} gives an estimate of the particle size. The spectroscopic properties of the particles are studied as a function of cadmium concentration and discussed in terms of particle size.

The effect of laponite clay interlayer space on intercalation of CdS has been investigated. Results indicate that the degree of "openness" of the interlayer space of the laponite film determines whether the intercalation of CdS in laponite film can occur. In these systems, solvents play the dominant role in opening the interlayer space. As methanol molecules cannot open the interlayer space sufficiently to allow S^{2-} anions to penetration into the clay, Cd is formed only on the external surface of the laponite–methanol systems. However, ethanol and 1-propanol molecules expand the layers sufficiently for CdS to form inside the interlayers. The minimum basal *d* spacing of an intercalated clay can be estimated from summation of the thickness of the tetrahedra–octahedra–tetrahedra sheet of clays and the diameters of guest molecules, if a monolayer of guest molecules is intercalated into the clay.

D. Silica–Alumina Catalysts

Photochemical reactions of pyrene on the surfaces of γ-alumina and silica–alumina have recently been investigated.[223] Pyrene molecules adsorb on these surfaces and form charge-transfer (CT) complexes at active sites of γ-alumina and silica–alumina which are formed by preheating the solids to an activation temperature, $T_a > 350$ °C. The latter exhibit absorption bands near the red edge of the characteristic absorption band of pyrene molecules. Pyrene excimer formation becomes significant on activated γ-alumina ($T_a < 300$ °C). Excited states of pyrene are quenched by surface states, leading to the formation of CT complexes. The radical cations formed on photoexcitation absorb strongly on the surfaces. These species exhibit a multilined EPR signal, while diffuse reflectance studies show that the radical cations also interact with parent molecules forming monopositive dimeric radical cations. The most interesting reaction of the radical cations on the surfaces is hydrolysis. The photochemical products on both activated and nonactivated surfaces were separated by HPLC, and the collected fractions were studied spectroscopically. The pH dependence of the absorption and fluorescence spectra taken together with results of mass spectrometry indicates that the main products are hydroxypyrenes. Water reacts with the radical cation forming the radical P(OH)*, which is a key intermediate in subsequent reactions.

XIII. Conclusion

The most basic difference between high-energy and low-energy excitation of systems is that the former excites the component of higher electron fraction, i.e., the bulk, and the latter excites selectively. For systems of solids with coadsorbed molecules, the high-energy radiation excites the solid structure, while photochemistry usually exites the solute exclusively.

For low-energy radiation the resulting chemistry is reminiscent of that seen in polar solvents, but on solids the movement of reactants is much lower than that in liquids. High-energy radiation produces ionization of the solid with subsequent transfer of excitation energy to the adsorbed solid. Ions and radicals of the adsorbate are formed, but adsorbate excited states are absent.

For both modes of excitation the resulting ion or free-radical chemistry is markedly affected by the topography of the surface.

High-energy radiation can produce chemistry in remote regions of solids, for example in the small cages of zeolites. Photochemistry is restricted to regions (large cages) where the adsorbate can penetrate. Hence, studies using both modes of excitation complement one another.

XIV. References

(1) The author wishes to thank NSF and EPA for support of this work.
(2) *An Introduction to Radiation Chemistry*; Spinks, J. W. T., Woods, R. J. J., Eds.; Wiley: New York, 1964.
(3) *Principles of Radiation Chemistry*; O'Donnell, J. H., Sangster, D. F., Eds.; E. Arnold: London, 1970.
(4) *Theoretical Foundations of Radiation Chemistry*; Bednar, J., Ed.; Kluwer Acad Press: Boston, 1990.
(5) *Chemistry of Excitation at Interfaces*; Thomas, J. K., Ed.; ACS Monograph 184; American Chemical Society: Washington, DC, 1984.
(6) *The Theory and Practice of Scintillation Counting*; Birks, J., Ed.; Pergamon Press: Oxford, 1964.
(7) Magee, J. L.; Huang, J. K. *J. Phys. Chem.* **1972**, *76*, 3801.
(8) Platzman, R. L. In *Radiation Research*; Silini, G., Ed.; North Holland: Amsterdam, 1967; p 20.
(9) Thomas, J. K. *Int. J. Radiat. Phys. Chem.* **1976**, *8*, 13.
(10) Beck, G.; Thomas, J. K. *J. Phys. Chem.* **1985**, *89*, 4062.
(11) Mezyk, S. P.; Yamamura, S.; Thomas, J. K. In *Radiation Effects in Polymers*; Clough, R. L., Shalaby, S., Eds.; ACS Symposium Series 475; American Chemical Society: Washington, DC, 1990; p 53.

(12) Krasnansky, R.; Koiche, K.; Thomas, J. K. *J. Phys. Chem.* **1990**, *94*, 4521.
(13) Kessler, R. W.; Oelkrug, D.; Wilkinson, F. *J. Appl. Spect.* **1982**, *36*, 673.
(14) Young, G. T. *J. Colloid Sci.* **1958**, *13*, 67.
(15) Anderson, J. H.; Lombard, J.; Haio, M. L. *J. Colloid Interface Sci.* **1975**, *50*, 519.
(16) de Mayo, P. *Pure Appl. Chem.* **1982**, *54*, 1623.
(17) Sler, R. K. *The Chemistry of Silica*; J. Wiley: New York, 1979; p 209–211.
(18) Hair, M. L.; Wertle, W. J. *J. Phys. Chem.* **1969**, *73*, 4269.
(19) Milosavljevic, B. J.; Thomas, J. K. *J. Phys. Chem.* **1988**, *92*, 2997.
(20) Sindoorf, D. W.; Maciel, G. E. *J. Am. Chem. Soc.* **1983**, *105*, 1487.
(21) Bronnimann, C. E.; Ziegler, R. C.; Maciel, G. E. **1988**, *110*, 2023.
(22) Sindoorf, P. W.; Maciel, G. E. *J. Phys. Chem.* **1982**, *86*, 5208.
(23) (a) Alkaitis, S. A.; Grätzel, M. *J. Am. Chem. Soc.* **1976**, *98*, 3549. (b) Hashimoto, S.; Thomas, J. K. *J. Phys. Chem.* **1984**, *88*, 4044.
(24) Peri, J. B.: Hannan, R. B. *J. Phys. Chem.* **1960**, *64*, 1526.
(25) Knözinger, H.; Ratnasamy, P. *Catal. Rev.-Sci. Eng.* **1981**, *17*, 31.
(26) Anderson, J. H.; Lombardi, J.; Hair, M. L. *J. Colloid Interface Sci.* **1975**, *50*, 519.
(27) Pohle, W. *J. Chem. Soc., Faraday Trans.* **1992**, *78*, 2101.
(28) Birks, J. B.; Shifkin, M. A. *Nature* **1961**, *191*, 761.
(29) Briegleb, G.; Czekalla, J. *J. Elektrochem.* **1959**, *63*, 6.
(30) Breck, D. W. *Zeolite Molecular Sieves*; J. Wiley: New York, 1974.
(31) Mottier, W. J. *Compilation of Extra-framework Sites in Zeolites*; Butterworth Scientific: Guildford, England, 1982.
(32) Calligaris, M.; Nardin, G.; Randoecio, L.; Zangrander, E. *Zeolite* **1986**, 439.
(33) McCusker, L.B.; Seff, K. *J. Phys. Chem.* **1981**, *85*, 166.
(34) Grim, R. E. *Clay Mineralogy*; McGraw Hill: New York, 1968.
(35) Van Olphen, H. *An Introduction to Clay Colloid Chemistry*, 2nd ed.; Wiley: New York, 1963.
(36) Thomas, J. M. *In intercalation Chemistry*; Whittingham, M.; Jacobson, A. L., Eds.; Academic Press: London, 1982.
(37) Theng, B. K. G. *The Chemistry of Clay-Organic Reactions*. Adam & Hegler: Melbourne, 1978.
(38) Barrer, R. M. *Philos. Trans. R. Soc. London A* **1984**, *311*, 333.
(39) Ballantine, J. A. In *Chemical Reactions in Organic and Inorganic Constrained Systems*; Setten, R., Ed.; Kluwer Academic publishers: Boston, 1989; p 197.
(40) Pinnavaia, T. J. Reference 39.
(41) Vaughan, D. E. V.; Lussier, R. Proc. 5th Int. Conf. Zeolites, Naples, p 94. Adams, P. A.; Thomas, J. M.; Jones, A.; Ballantine, J. A.; Purnell, H. *J. Chem. Soc., Chem. Commun.* **1984**, 1340.
(42) Van Olphen, H. *Clays Clay Miner.* **1954**, *2*, 418.
(43) Foster, W. R.; Savins, J. G.; Waite, J. M. *Clays Clay Miner.* **1954**, *3*, 246.
(44) Wood, W. H.; Grandquist, W. T.; Krieger, I. M. *Clays Clay Miner.* **1955**, *4*, 240.
(45) Cebula, D. J.; Thomas, R. K.; Middleton, S. R. *Clays Clay Miner.* **1979**, *27*, 39.
(46) Cebula, D. J.; Ottewell, R. H. *Clays Clay Miner.* **1981**, *29*, 13.
(47) Kuykendall, V. G.; Thomas, J. K. *Langmuir* **1990**, *6*, 1350.
(48) Viani, B. E.; Roth, C. B.; Low, P. F. *Clays Clay Miner.* **1985**, *33*, 244.
(49) Viani, B. E.; Low, P. F.; Roth, C. B. *J. Colloid Interface Sci.* **1983**, *96*, 229.
(50) Moyes, J. R. *Minerals Eng. Soc. Tech. Mag. (U. Birmingham)* **1975–1976**, *41–53*, 19.
(51) Laporte Industries, Technical Brochure no. L64.
(52) Kubelka, P.; Munk, F. *Z. Tech. Phys.* **1931**, *12*, 593.
(53) Kubelka, P. *J. Opt. Soc. Am.* **1948**, *38*, 448.
(54) Kortüm, G. *Reflectance Spectroscopy*; Springer-Verlag: Berlin, 1969.
(55) Stone, F. S. In *Surface Properties and Catalysis by Non Metals*; Bonnelle, J. P., Ed.; D. Reutal: Berlin, 1983; p 237.
(56) Oelkrug, D.; Honnen, W.; Wilkinson, F.; Willsher, C. J. *J. Chem. Soc., Faraday Trans. 2* **1987**, *83*, 2081.
(57) Wendlandt, W. W.; Hecht, H. G. *Reflectance Spectroscopy*; Interscience: New York, 1966.
(58) Alberty, W. J.; Bartlett, P. N.; Wilde, C. P.; Darwent, J. R. *J. Am. Chem. Soc.* **1985**, *107*, 1854.
(59) Scott, K. F. *J. Chem. Soc., Faraday Trans. 1* **1980**, *76*, 2065.
(60) Wolszczak, M.; Thomas, J. K. *Radiat. Phys. Chem.* **1991**, *38*, 155.
(61) Krasnansky, R.; Thomas, J. K. *J. Photochem. Photobiol. A.: Chem.* **1991**, *57*, 81.
(62) Krasnansky, R.; Koiche, K.; Thomas, J. K. *J. Phys. Chem.* **1990**, *94*, 4521.
(63) (a) Drake, J. M.; Levitz, P.; Turro, N. J.; Nitsche, K. S.; Cassidy, K. F. *J. Phys. Chem.* **1988**, *92*, 4680. (b) Samuel, J.; Ottolenghi, M.; Avnir, D. *J. Phys. Chem.* **1991**, *95*, 8440. (c) Tachiya, M. *J. Chem. Phys.* **1986**, *84*, 6178.
(64) *Molecular Dynamics in Restricted Geometries*; Klafter, J., Deake, J. M., Eds.; J. Wiley and Sons: New York, 1989.
(65) Klafter, J.; Deake, J. M.; Blumen, A. *J. Lumin.* **1984**, *31*, 642.
(66) Avnir, D.; Ottolenghi, M. In *Photochemistry in Organised and Contained Media*; Ramamurthy, V., Eds.; VCH: New York, 1991; p 535.
(67) Klafter, J.; Blumen, A. *J. Chem. Phys.* **1985**, *80*, 874.
(68) Pines, D.; Huppert, D.; Avnir, D. *J. Chem. Phys.* **1988**, *89*, 1177.
(69) deMayo, P.; Natarajam, L. V.; Ware, W. R. In *Organic Phototransformations in Nonhomogeneous Media*; Fox, M. A., Ed.; American Chemical Society: ACS Washington, 1985; p 1.
(70) Johnston, L. J. In *Photochemistry in Oranised and Constrained Media*; Ramamurthy, V., Ed.; VCH: New York, 1991; p 359.
(71) Scaiano, J. C.; Casal, H. L.; Netto-Perreira, J. C. Reference 69, p 211.
(72) Wilkinson, F. J. *J. Chem. Soc., Faraday 2* **1986**, *82*, 2073.
(73) Ramamurthy, V. Reference 70, p 429.
(74) Turro, N.; Garcia-GAribay, M. Reference 70, p 1.
(75) Thomas, J. K. *Acc. Chem. Res.* **1988**, *21*, 275.
(76) Suib, S. L. In *Photochemistry and Photophysics III*; Rabek, J., Ed.; CRC: Boca-Raton, 1991; p 1.
(77) (a) Chandratillake, M. R.; Newton, G. W. A.; Robinsen, V. J.; Rodgers, M. A. J. *Phys. Status Solidi B.* **1980**, *102*(2), 617. (b) Chandratillake, M. R.; Maliyadde, R.; Newton, G. W. A.; Robinsen, V. J.; Rodgers, M. A. J. *J. Chem. Soc., Faraday Trans. 2* **1977**, *73* (*12*), 1739. (c) Chandratillake, M. R.; Maliyadde, R.; Newton, G. W. A.; Patil, S. F.; Robinson, V. J.; Rogers, M. A. J. *J. Chem. Soc., Faraday Trans. 2* **1978**, *74* (*2*), 480.
(78) Grant, J. L.; Cooper, R.; Boas, J. F. *J. Chem. Phys.* **1988**, *80*, 4158.
(79) Caufield, K. J.; Cooper, R.; Boas, J. F. *J. Chem. Phys.* **1990**, *92*, 6441.
(80) Caffrey, J. M.; Allen, A. O. *J. Phys. Chem.* **1958**, *62*, 33.
(81) Kohn, H. W. *The Radiation Chemistry of Surfaces*. In *Actions Chimiques et Biologiques des Radiations (Chemical and Biological Action of Radiation)*; Masson & Cie: Paris, 1967.
(82) Wong, P. K.; Allen, A. O. *J. Phys. Chem.* **1970**, *74*, 774.
(83) Wong, P. K.; Willard, J. E. *J. Phys. Chem.* **1968**, *72*, 2623.
(84) Wong, P. K.; Willard, J. E. *J. Phys. Chem.* **1969**, *73*, 2226.
(85) Sagert, N. H.; Reid, J. A.; Robinson, R. W. *Can. J. Chem.* **1970**, *48*, 17.
(86) Toppien, G. R.; Willard, J. E. *J. Phys. Chem.* **1972**, *76*, 3158.
(87) Abrams, L.; Allen, A. O. *J. Phys. Chem.* **1969**, *73*, 2741.
(88) Rabe, J. G.; Rabe, B.; Allen, A. O. *J. Phys. Chem.* **1966**, *70*, 1098.
(89) Rojo, E. A.; Hentz, R. R. *J. Phys. Chem.* **1966**, *70*, 2919.
(90) Wong, P. K. *J. Phys. Chem.* **1971**, *75*, 201.
(91) Kazansky, V. B.; Pariisky, B. G.; Voevodssky, V. V. *Discuss. Farad. Soc.* **1961**, *31*, 203.
(92) Iler, R. K. The Chemistry of Silica Gel; Wiley: New York, 1979.
(93) Nelson, C. M.; Weeks, R. A. *J. Appl. Phys.* **1961**, *32*, 883.
(94) Weeks, R. A.; Fell, E. *J. Appl. Phys.* **1964**, *35*, 1932.
(95) Compton, W. D.; Arnold, G. W. *Discuss. Farad. Soc.* **1961**, *31*, 130.
(96) Arnold, G. W.; Compton, W. D. *Phys. Rev.* **1959**, *116*, 802.
(97) Levy, P. W. *J. Phys. Chem. Solids* **1960**, *13*, 287.
(98) Baxter, C.; Wagner, C. D. *J. Phys. Chem.* **1964**, *68*, 2381.
(99) Boreskov, G. K.; Kazananskii, V. B.; Yu, A.; Mishchenko, A.; Pariikii, G. B. *Dokl. Akar. Nauk SSSR* **1964**, *157*, 384.
(100) Devine, R. A. B. *Phys. Rev. Lett.* **1989**, *62*, 340.
(101) Tsai, T. E.; Griscom, D. L.; Friebele, E. J. *Phys. Rev. Letters* **1988**, *61*, 444.
(102) Wong, P. K.; Allen, A. O. *J. Phys. Chem.* **1970**, *74*, 774.
(103) Hentz, R. R.; Perkey, L. M.; Williams, R. H. *J. Phys. Chem.* **1966**, *70*, 731.
(104) Hentz, R. R.; Wickenden, D. K. *J. Phys. Chem.* **1969**, *73*, 813.
(105) Rojo, E. A.; Hentz, R. R. *J. Phys. Chem.* **1972**, *76*, 3741.
(106) Lee, S.; Bray, P. J. *Phys. Chem. Glasses* **1962**, *3*, 37.
(107) Stamires, D.; Turkevich, J. *J. Chem. Phys.* **1964**, *86*, 757.
(108) Iton, L. E.; Turkevich, J. *J. Phys. Chem.* **1978**, *82*, 200.
(109) Ksai, P. H. *J. Chem. Phys.* **1965**, *43*, 3323. Rabo, J. A.; Angell, C. L.; Kasai, P. H.; Schomaker, V. *Discuss. Faraday Soc.* **1966**, *41*, 328.
(110) Kasai, P. H.; Bishop, R. J. In *Zeolite Chemistry and Catalysis*; Rabo, J. A., Ed.; ACS Monograph 171, American Chemical Society: Washington, DC, 1976, p 350.
(111) Barrer, R. M.; Cole, F. J. *J. Phys. Chem. Solids* **1968**, *29*, 1755.
(112) Edwards, P. P.; Harrison, M. R.; Klinowski, J.; Ramdas, S.; Thomas, J. M.; Johnson, D. C.; Page, C. J. *J. Chem. Soc., Chem. Commun.* **1984**, 982.
(113) Harrison, M. R.; Edwards, P. P.; Klinowski, J.; Johnson, D. C.; Page, C. J. *J. Solid State Chem.* **1984**, *54*, 530.
(114) Westphal, U.; Geismar, G. Z. *Anorg. Allg. Chem.* **1984**, *508*, 165.
(115) Smeulders, J. B. A. F.; Hefni, M. A.; Klassen, A. A. K.; de Boer, E.; Westphal, U.; Geismar, G. *Zeolites* **1987**, *7*, 347.
(116) Breuer, R. E. H.; de Boer, E.; Geismar, G. *Zeolites* **1989**, *9*, 336.
(117) Yoon, K. B.; Kochi, J. K. *J. Chem. Soc., Chem. Commun.* **1988**, 510.
(118) Martens, L. R. M.; Grobet, P. J.; Jacobs, P. A. *Nature* **1985**, *315*, 568.
(119) Martens, L. R. M.; Grobet, P. J.; Vermerien, W. J. M.; Jacobs, P. A. *Proc. 7th Int. Zeolite Conf.*; Murakami, Y., Iigima, A., Ward, J. W., Eds.; Elsevier: New York, 1986; p 935.
(120) Martens, L. R. M.; Vermerien, W. J. M.; Grobet, P. J.; Jacobs, P. A. *Stud. Surf. Sci. Catal.* **1987**, *31*, 531.
(121) Anderson, P. A.; Edwards, P. P. *J. Chem. Soc., Chem. Commun.* **1991**, 915.
(122) Anderson, P. A.; Singer, R. J.; Edwards, P. P. *J. Chem. Soc., Chem. Commun.* **1991**, 914.

(123) Xu, B.; Kevan, L. *J. Chem. Soc., Faraday Trans.* **1991**, *87*, 2843.
(124) Haug, K.; Srdanov, V. I.; Voislav, D.; Stuckey, G.; Metin, H. *J. Chem. Phys.* **1992**, *96*, 3495.
(125) Nakagato, C.; Masuda, T. *Bull. Chem. Soc. Jpn.* **1986**, *59*, 2237.
(126) Aoki, M.; Nakazato, C.; Masuda, T. *Bull. Chem. Soc. Jpn.* **1988**, *61*, 1899.
(127) deMayo, P.; Okada, K.; Rafalska, M.; Weedon, A. C.; Wong, G. S. K. *J. Chem. Soc., Chem. Commun.* **1981**, 820.
(128) Bauer, R. K.; Borenstein, R.; deMayo, P.; Okada, K.; Rafalska, M.; Ware, W. R.; Wu, K. C. *J. Am. Chem. Soc.* **1982**, *104*, 4635.
(129) Bauer, R. K.; deMayo, P.; Ware, W. R.; Wu, K. C. *J. Phys. Chem.* **1982**, *86*, 3781.
(130) Hara, K.; deMayo, P.; Ware, W. R.; Waden, A. L.; Wong, G. S. K.; Wu, K. C. *Chem. Phys. Lett.* **1980**, *69*, 105.
(131) Avnir, D.; deMayo, P.; Ono, I. *J. Chem. Soc., Chem. Commun.* **1968**, 1109.
(132) Avnir, D.; Johnston, L. J.; deMayo, P.; Wong, S. K. *J. Chem. Soc., Chem. Commun.* **1981**, 958.
(133) Eorcinov, V. L.; Golubreu, V. G.; Luneona, Z. V. *Russ. J. Phys. Chem. (Engl. Transl.)* **1975**, *49*, 564.
(134) Selevanowski, A. K. *Russ. J. Phys. Chem. (Engl. Transl.)* **1976**, *50*, 990.
(135) Frederick, B.; Johnson, L. J.; deMayo, P.; Wong, S. K. *Can. J. Chem.* **1984**, *61*, 403.
(136) deMayo, P.; Nakamura, A.; Tsang, P. N. K.; Wong, S. K. *J. Am. Chem. Soc.* **1982**, *104*, 6824.
(137) Nakashima, H.; Phillips, D. *Chem. Phys. Letts.* **1983**, *97*, 337.
(138) Kessler, R. W.; Wilkinson, F. *J. Chem. Soc., Faraday Trans. 1* **1977**, *77*, 309.
(139) Wilkinson, F.; Willsher, C. *J. Chem. Phys. Lett.* **1984**, *104*, 272.
(140) Ferguson, J. *J. Chem. Phys.* **1985**, *28*, 765.
(141) Wong, A. L.; Harris, J. M. *J. Phys. Chem.* **1991**, *95*, 5895. Wong. A. L.; Hunnicutt, M. L.; Harris, J. M. *J. Phys. Chem.* **1991**, *95*, 4489.
(142) Silva, S.; Olea, A. F.; Thomas, J. K. *Photochem. Biotobiol.* **1991**, *54*, 511.
(143) Turro, N. J.; Zimmt, M. B.; Gould, I. R. *J. Am. Chem. Soc.* **1985**, *107*, 5826.
(144) Oelkrug, D.; Uhl, S.; Wilkinson, F.; Willsher, C. J. *J. Phys. Chem.* **1989**, *93*, 4551.
(145) Oelkrug, D.; Gregor, M.; Rach, S. *Photochem. Photobiol.* **1991**, *54*, 539.
(146) Oelkrug, D.; Uhl, S.; Gregor, M.; Lege, R.; Kelley, G.; Wilkinson, F. *J. Mol. Struct.* **1990**, *218*, 435.
(147) Hite, P.; Krasnansky, R.; Thomas, J. K. *J. Phys. Chem.* **1986**, *90*, 5795.
(148) Krasnansky, R.; Thomas, J. K. *J. Photochem. Photobiol., A: Chem.* **1991**, *57*, 81.
(149) (a) Hair, M. L.; Herl, W. J. *J. Phys. Chem.* **1969**, *73*, 4269. (b) Marro, M.; Thomas, J. K. Unpublished work.
(150) Turro, N. J. *Tetrahedron* **1987**, *43*, 1589. deMayo, P.; Johnson, L. J. In *Preparative Chemistry Using Supported Reagents*; Taszolo, P., Ed.; Acad. Press: San Diego, 1987; Chapter 4.
(151) Frederick, B.; Johnson, L. J.; deMayo, P.; Wong, S. K. *Can. J. Chem.* **1984**, *62*, 403.
(152) Turro, N. J.; Baretz, B. H. *J. Am. Chem. Soc.* **1983**, *105*, 1310.
(153) Johnson, L. J. In *Photochemistry in Organised and Constrained Media*; V. Ramamurthy, V., Ed.; VCH Publ: New York, 1991; p 364.
(154) Wong, P. K. *Photochem. Photobiol.* **1974**, *19*, 391.
(155) Tanci, T. *Bull. Chem. Soc. Jpn.* **1968**, *41*, 833.
(156) Wilkinson, F.; Willsher, C. J.; Uhl, S.; Honnen, W.; Oelkrug, D. J. *Photochemistry* **1986**, *33* (*3*), 273.
(157) Oelkrug, D.; Flemming, W.; Fullemann, R.; Günther, R.; Honne, W.; Krabichler, G.; Schäfer, M.; Uhl, S. *Pure Appl. Chem.* **1986**, *58*, 1207.
(158) Thomas, J. K. *J. Phys. Chem.* **1987**, *91*, 267.
(159) Oelkrug, D.; Radjaiopour, M.; Erbse, H. *Z. Phys. Chem. Neue Folge* **1974**, *88*, 23.
(160) Oelkrug, D.; Erbse, H.; Plauschinat, M. *Z. Phys. Chem. Neue Folge* **1975**, *96*, 283.
(161) Oelkrug, D.; Schrem, G.; Andrä, I. *Z. Phys. Chem. Neue Folge* **1977**, *106*, 197.
(162) Oelkrug, D.; Plauschinat, M.; Kessler, R. W. *J. Lumin.* **1979**, *18/19*, 434.
(163) Oelkrug, D.; Radjaiopour, M. *Z. Phys. Chem. Neue Folge* **1980**, *123*, 163.
(164) Kessler, R. W.; Uhl, S.; Honnen, W.; Oelkrug, D. *J. Lumin.* **1981**, *24/25*, 551.
(165) Kessler, R. W.; Oelkrug, D.; Uhl, S. *Vide, Couches Minces* **1981**, *209*, 1334.
(166) Uhl, S.; Oelkrug, D. *J. Mol. Struct.* **1988**, *175*, 117.
(167) Kessler, R. W.; Krabichler, G.; Uhl, S.; Oelkrug, D.; Hagan, W. G.; Hyslop, J.; Wilkinson, F. *Optica Acta* **1983**, *30*, 1099.
(168) Honnen, W.; Krabichler, G.; Uhl, S.; Oelkrug, D. *J. Mol. Struct.* **1984**, *115*, 351.
(169) Rempfer, K.; Uhl, S.; Oelkrug, D. *J. Mol. Struct.* **1984**, *114*, 225.
(170) Honnen, W.; Krabichler, G.; Uhl, S.; Oelkrug, D. *J. Phys. Chem.* **1983**, *87*, 4872.
(171) Uhl, S.; Krabichler, G.; Rempfer, K.; Oelkrug, D. *J. Mol. Struct.* **1986**, *143*, 279.
(172) Oelkrug, D.; Krabichler, G.; Honnen, W.; Wilkinson, F.; Willsher, C. J. *J. Phys. Chem.* **1988**, *92*, 3589.
(173) Oelkrug, D.; Reich, S.; Wilkinson, F.; Leicester, P. A. *J. Phys. Chem.* **1991**, *95*, 269.
(174) (a) Asmolov, G. N.; Krylov, O. V. *Kinet. Katal.* **1978**, *19*, 975. (b) Asmolov, G. N.; Krylov, O. V. *Kinet. Katal.* **1978**, *19*, 979.
(175) Pankasem, S.; Thomas, J. K. *J. Phys. Chem.* **1991**, *95*, 6990.
(176) Pankasem, S.; Thomas, J. K. *J. Phys. Chem.* **1991**, *95*, 7385.
(177) Pankasem, S.; Thomas, J. K. *Langmuir* **1992**, *8*, 501.
(178) Gijzman, O. L.; Kaufman, F.; Porter, G. *J. Chem. Soc., Faraday Trans. 2* **1973**, *69*, 708.
(179) Bech, G.; Thomas, J. K. *Chem. Phys. Lett.* **1983**, *94*, 553.
(180) Debye, P.; Edwards, J. O. *J. Chem. Phys.* **1952**, *20*, 236.
(181) Abell, G.; Mozumder, A. *J. Chem. Phys.* **1972**, *56*, 4079.
(182) Slama-Schwok, A.; Avnir, D.; Ottolenghi, M. *J. Phys. Chem.* **1989**, *93*, 7544.
(183) Birenbaum, H.; Avnir, D.; Ottolenghi, M. *Langmuir* **1989**, *5*, 48.
(184) Liu, X.; Iu, K. K.; Thomas, J. K. *J. Phys. Chem.* **1989**, *93*, 4120.
(185) Iu, K. K.; Thomas, J. K. *Langmuir* **1990**, *6*, 471.
(186) Iu, K. K.; Liu, X.; Thomas, J. K. *Mat. Res. Soc.* **1991**, *223*, 119.
(187) Dinesenko, G. I.; Lisovenko, V. A. *Zl. Prikl Spektrosk.* **1971**, *14*, 702.
(188) Incavo, J. A.; Dutta, P. K. *J. Phys. Chem.* **1990**, *94*, 3075.
(189) Baretz, B. H.; Turro, N. J. *J. Photochem.* **1984**, *24*, 201.
(190) Milosavljevic, B. H.; Thomas, J. K. *J. Phys. Chem.* **1985**, *89*, 1830; *J. Am. Chem. Soc.* **1986**, *108*, 2513.
(191) Yoon, K. B.; Kochi, J. K. *J. Am. Chem. Soc.* **1989**, *111*, 1128.
(192) Sanakararaman, S.; Yoon, K. B.; Yabe, T.; Kochi, J. K. *J. Am. Chem. Soc.* **1991**, *113*, 1419.
(193) Tachiya, M.; Mozumder, A. *Chem. Phys. Lett.* **1974**, *28*, 87.
(194) Iu, K. K.; Thomas, J. K. *J. Phys. Chem.* **1991**, *95*, 506; *Colloids Surf.* **1992**, *63*, 39.
(195) Liu, X.; Thomas, J. K. *Chem. Phys. Lett.* **1992**, *192*, 555.
(196) Iu, K. K.; Liu, X.; Thomas, J. K. Unpublished results.
(197) Liu, X.; Thomas, J. K. *Langmuir* **1989**, *5*, 58.
(198) Wang, Z.; Herron, H. *J. Phys. Chem.* **1987**, *91*, 257.
(199) Moller, K.; Eddy, M. M.; Stucky, G. D.; Herron, N.; Bien, T. *J. Am. Chem. Soc.* **1989**, *111*, 2564.
(200) Stramel, R.; Nakamura, T.; Thomas, J. K. *J. Chem. Soc., Faraday Trans Soc. 1* **1988**, *84*, 1287.
(201) Liu, X.; Thomas, J. K. *Chem. Phys. Lett.* **1988**, *144*, 286.
(202) Ozin, G. A.; Hugues, F.; Mattar, S. M. *J. Phys. Chem.* **1985**, *89*, 305.
(203) Beer, R.; Calzaferri, G.; Li, J.; Waldeck, B. *Coord. Chem. Rev.* **1991**, *111*, 193. Calzaferri, G.; Foss, L. *Helv. Chim. Acta* **1986**, *69*, 873; **1987**, *70*, 1485.
(204) Chandrasekaran, K.; Thomas, J. K. *Chem. Phys. Lett.* **1983**, *97*, 357.
(205) Dellaguardia, R.; Thomas, J. K. *J. Phys. Chem.* **1983**, *87*, 3550.
(206) Dellaguardia, R.; Thomas, J. K. *J. Phys. Chem.* **1984**, *88*, 964.
(207) Nakamura, T.; Thomas, J. K. *Langmuir* **1985**, *1*, 568.
(208) Nakamura, T.; Thomas, J. K. *Langmuir* **1986**, *90*, 641.
(209) Vianene, K.; Schoolheydt, R. A.; Critzen, M.; Kunyima, B.; DeSchryver, F. *Langmuir* **1988**, *4*, 749.
(210) Kuykendall, V. G.; Thomas, J. K. *J. Phys. Chem.* **1990**, *94*, 4224.
(211) Kuykendall, V. G.; Thomas, J. K. *Langmuir* **1990**, *6*, 1350.
(212) Jones, W. Reference 70; p 37.
(213) Thomas, J. M. *Intercalation Chemistry*; Whittingham, M. S., Jacobson, A. J., Eds.; Academic Press: London, 1982; p 55.
(214) Barrer, R. M. *Zeolites and Clay Minerals as Sorbents and Molecular Sieves*; Acad. Press: London, 1978.
(215) Liu, X.; Thomas, J. K. *Langmuir* **1991**, *7*, 2808.
(216) Iu, K. K.; Liu, X.; Thomas, J. K. *Chem. Phys. Lett.* **1991**, *186*, 198.
(217) Liu, X.; Iu, K. K.; Thomas, J. K. *Langmuir* **1992**, *8*, 539.
(218) Pankasem, S.; Liu, X.; Thomas, J. K. *J. Photochem. Photobiol. A* **1991**, *62*, 53.
(219) Stramel, R. D.; Nakamura, T.; Thomas, J. K. *Chem. Phys. Lett.* **1986**, *130*, 423.
(220) Stramel, R. D.; Nakamura, T.; Thomas, J. K. *J. Chem. Soc., Faraday Trans. 1* **1988**, *84*, 1287.
(221) Liu, X.; Iu, K. K.; Thomas, J. K. *J. Colloid Interface Sci.* **1989**, *129*, 476.
(222) Kuczynski, J.; Thomas, J. K. *J. Phys. Chem.* **1985**, *89*, 2720.
(223) Mao, Y.; Thomas, J. K. *Langmuir*, in press; *J. Chem. Soc., Faraday Trans.* **1992**, *88*, 3079.